

NEUTRON STAR POPULATION DYNAMICS.II: 3D SPACE VELOCITIES OF YOUNG PULSARS

J. M. Cordes

Astronomy Department and NAIC, Cornell University

David F. Chernoff

Astronomy Department, Cornell University

ABSTRACT

We use astrometric, distance and spindown data on pulsars to: (1) estimate three-dimensional velocity components, birth distances from the galactic plane, and ages of individual objects; (2) determine the distribution of space velocities and the scale height of pulsar progenitors; (3) test spindown laws for pulsars; (4) test for correlations between space velocities and other pulsar parameters; and (5) place empirical requirements on mechanisms than can produce high velocity neutron stars. Our approach incorporates measurement errors, uncertainties in distances, deceleration in the Galactic potential, and differential galactic rotation. We focus on a sample of proper motion measurements of young pulsars (< 10 Myr) whose trajectories may be accurately and simply modeled. This sample of 47 pulsars excludes millisecond pulsars and other objects that may have undergone accretion-driven spinup.

We estimate velocity components and birth z distance on a case-by-case basis assuming the actual age equals the conventional spindown age for a braking index $n=3$, no torque decay, and birth periods much shorter than present day periods. Every sample member could have originated within 0.3 kpc of the galactic plane while still having reasonable present day peculiar radial velocities.

For the 47-object sample, the scale height of the progenitors is ~ 0.13 kpc and the three dimensional velocities are distributed in two components with characteristic speeds of 175_{-30}^{+20} km s $^{-1}$ and 700_{-150}^{+200} km s $^{-1}$, representing $\sim 83\%$ and $\sim 17\%$ of the population, respectively. The sample velocities are inconsistent with a single component Gaussian model, well-described by a two component Gaussian model but do not require models of additional complexity. From the best-fit distribution, we estimate that about 20% of the known pulsars will escape the Galaxy, assuming an escape speed of 500 km s $^{-1}$. The best-fit, dual-component model, if augmented by an additional, low velocity (< 50 km s $^{-1}$) component tolerates, at most, only a small extra contribution in number,

less than 5%. The best three component models do not show a preference for filling in the probability distribution at speeds intermediate to 175 and 700 km s^{-1} but are nearly degenerate with the best two component models. We estimate that the high velocity tail ($> 1000 \text{ km s}^{-1}$) may be underrepresented by a factor ~ 2.3 owing to selection effects in pulsar surveys.

The estimates of scale height and velocity parameters are insensitive to the explicit relation of chronological and spindown ages. A further analysis starting from our inferred velocity distribution allows us to test spindown laws and age estimates. There exist comparably good descriptions of the data involving different combinations of braking index and torque decay timescale. We find a braking index of 2.5 is favored if torque decay occurs on a time scale of $\sim 3 \text{ Myr}$, while braking indices between 3.5 and 6 are preferred if there is no torque decay. For the sample as a whole, the most-probable chronological ages are typically smaller than conventional spindown ages by factors as large as two.

We have also searched for correlations between three-dimensional speeds of individual pulsars and combinations of spin period and period derivative. None appears to be significant. We argue that correlations identified previously between velocity and (apparent) magnetic moment reflect the different evolutionary paths taken by young, isolated (nonbinary), high-field pulsars and older, low-field pulsars that have undergone accretion-driven spinup. We conclude that any such correlation measures differences in spin and velocity selection in the *evolution* of the two populations and is not a measure of processes taking place in the core collapse that produces neutron stars in the first place.

We assess mechanisms for producing high-velocity neutron stars, including disruption of binary systems by symmetric supernovae and neutrino, baryonic or electromagnetic rocket effects during or shortly after the supernova. The largest velocities seen ($\sim 1600 \text{ km s}^{-1}$) along with the paucity of low-velocity pulsars suggest that disruption of binaries by symmetric explosions is insufficient. Rocket effects appear to be a necessary and general phenomenon. The required kick amplitudes and the absence of a magnetic-field-velocity correlation do not yet rule out any of the rocket models. However, the required amplitudes suggest that the core collapse process in a supernova is highly dynamic and aspherical and that the impulse delivered to the neutron star is larger than existing simulations of core collapse have achieved.

Subject headings: pulsars, stars-binary:

1. INTRODUCTION

The high velocity nature of pulsars has been recognized since the first, minimal sample was analyzed by Gunn & Ostriker (1970). As pulsar discoveries and proper-motion measurements have increased, and the pulsar distance scale improved, the largest inferred velocity has increased to $\gtrsim 1000 \text{ km s}^{-1}$. The population’s dispersion exceeds that of any other normal Galactic stellar population.

Although it is likely that a pulsar’s characteristic motion is generated during the neutron star formation, a number of physical mechanisms has been proposed. In broad terms, these include: (1) disruption of binaries through instantaneous, symmetric mass loss in supernova explosions (Blaauw 1961; Gott, Gunn & Ostriker 1970; Radhakrishnan & Shukre 1985); (2) slow, post-explosion, rocket effects associated with loss of spin energy by the neutron stars (e.g. Harrison & Tademaru 1975; Helfand & Tademaru 1977); and (3) an instantaneous momentum impulse, or “kick”, imparted through asymmetry of the supernova explosion (Shklovskii 1970; Dewey & Cordes 1987).

Many statistical analyses of pulsar velocities have attempted to discern which (if any) of the mechanisms is favored (Dewey & Cordes 1987; Bailes 1989; Iben & Tutukov 1996). The recent treatment by Lyne & Lorimer (1994; hereafter LL) has incorporated new proper-motion measurements (Harrison *et al.* 1993) and an up-to-date model for the free electron density in the Galaxy (Taylor & Cordes 1993; hereafter TC). The latter is essential for estimating distances to most pulsars. LL find a larger mean pulsar speed, $\bar{V} \sim 450 \text{ km s}^{-1}$, than had been estimated previously. The probability density function (pdf) for the perpendicular speed is

$$f_{V_{\perp}}(V_{\perp}) \propto \frac{(V_{\perp}/V_0)^{0.3}}{1 + (V_{\perp}/V_0)^{3.3}}, \quad (1)$$

where $V_0 = 330 \text{ km s}^{-1}$ (and $dN \propto f_{V_{\perp}} d^2V_{\perp}$)¹. LL state that $\sim 50\%$ of pulsars will escape the Galaxy, assuming an escape speed $\sim 500 \text{ km s}^{-1}$. LL also re-emphasized the fact that pulsar surveys tend to undercount the highest velocity pulsars. Surveys are signal-to-noise limited and sample a finite volume which, of course, is roughly centered on the Galactic plane. Since it is generally thought that most pulsars are born in the vicinity of the Galactic plane and move away from it, fast objects spend less time in the detectable volume than slow ones and are consequently under-represented.

In attempting to characterize the pulsar velocity distribution, a fundamental difficulty is that *all* of the basic components necessary for a kinematic description of the population

¹The given expression corrects a typographical error in LL, according to Mollerbach & Roulet (1997)

are poorly known. Except for a few historical supernovae, the *chronological age* of each individual object is unknown and it must be estimated from the “spindown” age. The *distance* is uncertain, though it may be constrained by a pulsar’s dispersion measure (DM) from knowledge of the electron density within the Galaxy. The perpendicular components of the *velocity* may be derived from the proper motion and distance, though the proper motion measurements only exist for a subset of the entire pulsar population and both distance and proper motion determinations have significant errors. In summary, there are significant uncertainties in the age, distance and velocity of nearly every known pulsar.

Our general goal is to infer properties, like the distribution of kick velocities at birth, for the pulsar population. Since there is no *a priori* way to separate the uncertainties we must strive to treat them in an even-handed, consistent manner. Although we do not completely fulfill that goal in this paper, we make significant progress by incorporating the uncertainties in position and velocity directly into our analysis and by separately considering the sensitivity of the results to the relation between spindown and chronological age. Our major omission, which we plan to treat in the future, is the observational selection effects associated with the detection problem itself. In effect, the observer’s selection function involves kinematic, geometric and detection-related pieces and we omit the last, focusing purely on the kinematic and geometric aspects.

In this paper we present a new analysis of pulsar velocities that (1) tests and exploits the hypothesis that pulsars are born in or near the plane of the Galaxy; (2) takes into account the uncertainties in pulsar distances and proper-motion measurements; (3) estimates the full three dimensional velocity pdf and birth scale height of the known pulsars; (4) uses the global information to sharpen the estimate of measured kinematic quantities and to infer the most likely values of other unmeasured quantities for each pulsar; and (5) constrains the braking index and torque decay time for pulsar spindown. Our methodology uses a likelihood analysis, augmented by a comparison of models with different complexity using Bayesian odds ratios. This paper is the second paper in a series, where the first addressed the population of millisecond pulsars, finding them to be a low-velocity population with rms velocity $\sim 84 \text{ km s}^{-1}$ (Cordes & Chernoff 1997; hereafter Paper I).

The first half of the paper deals directly with the statistical procedures we have developed and the application to the data. In §2 we describe the selection criteria for the pulsar sample. §3 outlines and applies our procedure for constraining radial velocities and birth altitudes for individual objects. §4 derives a best fit three dimensional velocity distribution for the population and discuss the kinematic constraints on the braking index. §5-7 use the statistical results as an aid in estimating separate velocity components, birth z and ages for individual pulsars. Using the estimated velocities we discuss in §8 the

velocity-magnetic moment correlation. §9 relates recent work on pulsar-supernova remnant associations to our analysis of the proper motion sample.

The second half of the paper relates our work to a number of topics of current astrophysical interest. In §10 we review the lines of evidence for asymmetric supernova kicks and derive the fraction of the observed sample that will escape the Galaxy. We discuss the form of the velocity distribution function and give arguments that suggest that kicks $\gtrsim 50 \text{ km s}^{-1}$ *always* occur and that a significant fraction of objects are moving so fast that *only* strong supernova kicks can explain their motion. We speculate about the relationship of the shape of the velocity distribution function to binary evolution scenarios. We discuss the implications for core collapse, drawing attention to the breaking of symmetry implied by the observed kick size.

Finally, we include a discussion of the search for the highest velocity objects in §11. We summarize our results in §12. Individual objects with idiosyncratic distance estimates or with extreme birth velocities or z altitudes are discussed in Appendix A.

2. PULSAR SAMPLE

The observables we use to analyze pulsar space velocities are the spin period and its first time derivative (P and \dot{P}); galactic coordinates (ℓ, b); the dispersion measure (DM); and the proper motions in the directions of right ascension and declination ($\mu_{\text{RA}}, \mu_{\text{DEC}}$) and their associated measurement errors ($\sigma_{\mu_{\text{RA}}}, \sigma_{\mu_{\text{DEC}}}$). We incorporate auxiliary information on particular lines of sight that includes the scattering measure (SM) and the locations of HII regions that may perturb distance estimates based on DM. The distance scale is based on the electron density model of TC, augmented by neutral hydrogen (HI) absorption measurements and other independent constraints on the distances, including 2 parallax measurements. In aggregate, the available data provide a formal distance estimate and, for most objects, lower and upper bounds (D_L, D_U) such as those presented by Frail (1990), Frail & Weisberg (1990) and Koribalski *et al.* (1995) based on HI absorption measurements, pulsar associations with supernova remnants, and parallax measurements.

Table 1 lists the data that we have used, which results from the requirement that the spindown age ($P/2\dot{P}$ for braking index $n = 3$ and no torque decay) be less than 10 Myr and that the distance estimate include a lower and upper bound. A chronological age cutoff is necessary because we treat the orbital motion of the pulsar analytically by a Taylor series approximation and this ceases to be accurate once significant changes in the acceleration have occurred. We focus on the *vertical* pulsar motion in our analysis ignoring all variations

with Galactocentric radius. We choose the age cutoff of 10 Myr to guarantee that virtually all bound objects are still in the first quarter cycle of their oscillation perpendicular to the galactic plane. As we discuss in more detail below, the 10 Myr age cutoff assures quite accurate vertical solutions in an infinite, planar Galaxy. However, in 10 Myr a 1000 km/s pulsar moves ~ 10 kpc, so the assumption of uniformity in the plane is nontrivial.

For each object the chronological age is based on P , \dot{P} and a spindown model. It turns out that the models of greatest interest have $n > 3$ and/or torque decay. For them, the chronological age is less than $P/2\dot{P}$ so the imposed cutoff of 10 Myr is more conservative than need be the case. Even for $2 < n < 3$, the maximum chronological age of 20 Myr degrades but does not destroy the accuracy of the vertical solution. The age cut implies that our sample excludes millisecond pulsars and other pulsars that may have undergone accretion-driven spinup, a process that necessarily is slow and is therefore manifested in older objects.

Of 96 objects with proper motion measurements, 47 satisfy our age and distance criteria. The 49 excluded objects include 45 that are older than 10 Myr, of which 18 are older than 100 Myr. An additional 4 objects were excluded because the TC distance model yielded only a lower bound on the distance and there was no auxiliary information to provide better constraints on the distance. The sample of 47 objects includes three with parallax measurements (B0630+17 [Geminga], Caraveo *et al.* 1996; B0823+26, Gwinn *et al.* 1986; and B2021+51, Campbell *et al.* 1996).

3. RADIAL VELOCITIES AND BIRTH ALTITUDES

We first derive constraints on the radial velocity and birth altitude, z_0 , from measurements of proper motion and distances on individual objects. In so doing, we demonstrate that all pulsars with measured proper motions are consistent with birth near the galactic plane, $|z_0| \lesssim 0.3$ kpc. This kind of analysis was first applied by Helfand & Tadamaru (1977) to a sample of 12 objects. Our conclusion about pulsar birth in the galactic disk is identical to that of Helfand & Tadamaru. Similarly, we find that the *apparent* motion of a few pulsars toward the galactic plane is due exclusively to projection effects. We extend previous analyses by taking into account errors on estimated distances and proper motions, acceleration in the galactic potential and alternative values for the braking index.

In the following, we review the age uncertainty and describe a model which incorporates an arbitrary braking index and torque decay. We outline the geometric relations that exist

between the estimated distance, proper-motion components, z-distance from the Galactic plane, z-value at birth, radial velocity and pulsar age. We formulate a likelihood function for a quantity composed of possible z-values at birth and peculiar radial velocities today. We compare its value on a case-by-case basis to *a priori* expectations.

3.1. Age Estimate Uncertainties

The spindown age for an object with period P and period derivative \dot{P} is defined as

$$\tau_S \equiv \frac{P}{(n-1)\dot{P}} \quad (2)$$

where n is the braking index. We have $n = 3$ for braking by radiation from a point magnetic dipole of constant strength. If n is a known constant, $n > 1$, and the initial period $P_0 \ll P$ then the spindown age τ_S and the chronological age t agree.

Measured braking indices are smaller than the dipole result: $n = 2.28$ for PSR B0540-69 (Boyd *et al.* 1995); $n = 2.51$ for the Crab pulsar (Lyne, Pritchard & Smith 1988); and $n = 2.83$ for PSR B1509-58 (Manchester *et al.* 1985; Kaspi *et al.* 1994). Most pulsars are much older than these objects and their braking indices cannot be measured reliably because timing irregularities mask the contribution from the small expected second period derivative, \ddot{P} . Work below indicates that values of the braking index $n \lesssim 3$ (and no torque decay) are less consistent with the kinematic data than are values $\gtrsim 3$ (and/or torque decays on a time scale of a few million years). Since most of the pulsars in our sample are significantly older than those for which braking indices have been measured directly, these facts imply that braking indices are not constant and/or torque decay is significant over a pulsar’s lifetime.

In principle, many physical effects can alter spindown from the static magnetic dipole limit. The strength of the magnetic field may change: Ohmic decay (Ostriker and Gunn 1969) and field growth (e.g. by thermal effects, Blandford, Applegate and Hernquist 1983) are both possible. Particle emission processes may be more important than dipole radiation in angular momentum loss (Michel 1969, Goldreich and Julian 1970) and the losses might scale differently with frequency and with magnetic field than dipole losses. The dipole geometry may change in time: some systematic changes in the relative orientation of the spin axis and the dipole axis were observationally inferred from the shape of pulsar beams (Lyne & Manchester 1988). The effective size of the dipole may change in time (Melatos 1997). Surface fields (as opposed to the field at the light cylinder) may be altered by mass accretion (Romani 1990) and crustal plate motion (Ruderman 1991); whether such changes influence the spindown rate is unclear.

It is difficult to test these ideas directly since measurement of torque decay may be masked by other physical processes occurring inside the neutron star. Some information is available. General observational indications are that pulsars that are or were members of binaries have weak fields of $10^8 - 10^9$ G that do not decay over lifetimes of $10^9 - 10^{10}$ yrs. In a number of recent, specific analyses involving accretion in binary systems field decay has been inferred to occur (e.g. Burderi, King & Wynn 1996). Current statistical studies of pulsar properties do not find strong evidence for field decay in single pulsars (e.g. van den Heuvel 1993) nor for changes in the relative orientation of spin and dipole axes (Bhattacharya & van den Heuvel 1991). Recently, Wang (1997) has argued that an isolated pulsed X-ray source accreting from the interstellar medium must have undergone field decay from $\sim 10^{12}$ G to 10^{10} G in $\sim 10^7$ yrs (by power law decay) or $\sim 10^8$ yrs (by exponential decay).

In view of the uncertainties, we adopt a phenomenological approach and write $\dot{\Omega} = -K(t)\Omega^n$, where t is the chronological age and $K(t)$ describes any time dependence of the torque law other than a pure power of the spin rate (“torque decay”). Most discussions on torque decay refer explicitly to exponential decay of the magnetic field for $n = 3$. Then $K(t) \propto B^2$, and the quoted *field* decay time is twice that of the torque decay. The notion of magnetic field decay has changed considerably since it was first introduced in discussions of pulsar evolution. Ohmic decay in the neutron star crust was initially thought to be fast enough to account for the turn-off of radio emission from pulsars (Gunn & Ostriker 1970) but it is now regarded as too slow to be relevant (e.g. Goldreich & Reisenegger 1992). For our uses, the phenomenological model applies for any $n > 1$ but the relation between B field and $K(t)$ will vary.

For exponential torque decay, $K(t) \propto \exp(-t/\tau_K)$ and the chronological age is given by (Bailes 1989)

$$t = \tau_K \ell n \left\{ 1 + \frac{\tau_S}{\tau_K} \left[1 - \left(\frac{P_0}{P} \right)^{n-1} \right] \right\}. \quad (3)$$

If $t \ll \tau_K$ and $P \gg P_0$, then $t \sim \tau_S$. In other words, the spindown age and the chronological age agree when the torque decay has not taken place and when the initial period is short compared to the current period. On the other hand, if $t \gtrsim \tau_K$ or if $P \sim P_0$, then $t \ll \tau_S$ implying that the spindown age overestimates the chronological age.

A braking index may be inferred from the instantaneous rate of change of frequency. The *estimated* braking index is

$$\hat{n} \equiv \frac{\ddot{\Omega}\Omega}{\dot{\Omega}^2} = n + (n - 1) \frac{\tau_S}{\tau_K}. \quad (4)$$

For $\tau_S \ll \tau_K$, $\hat{n} = n$ but for $\tau_S \gtrsim \tau_K$ and $n > 1$, $\hat{n} > n$. This sort of evolution would

be consistent with both the small measured values of \hat{n} for very young pulsars and the larger kinematically inferred values of \hat{n} for older objects (see below, §4.5, where we discuss constraints on spindown laws).

3.2. Coordinates, Kinematic and Peculiar Velocities, & Proper Motions

We adopt U, V, W coordinates (Mihalas & Binney 1981, pp. 382-383) where U and V point toward $\ell = 180^\circ$ and $\ell = 90^\circ$, respectively, for $b = 0$ and W points toward $b = 90^\circ$. We transform the measured proper motions and their errors to the UVW system to obtain $\mu_{U,V,W}$ and $\sigma_{\mu_{U,V,W}}$.

Let z be the present distance from the plane, z_0 be the distance at birth from the plane² and \ddot{z} be the acceleration at the current position. The present-day, “kinematic” z velocity of an object of age t is

$$V_z \approx \frac{z - z_0}{t} + \frac{\ddot{z}t}{2} \quad (5)$$

and the birth z velocity is

$$V_{z0} \approx V_z - \ddot{z}t. \quad (6)$$

The Taylor series expansion is accurate for pulsars younger than $\sim 1/4$ their z -oscillation period. Figure 1 shows $V_z(t)$ for pulsars with $z_0 = 0$ moving in a three-component model for the galactic potential (Paczynski 1990). The very slowest pulsars (e.g. $V_{z0} \lesssim 10 \text{ km s}^{-1}$), have asymptotic periods of 60-70 Myr (near the Sun), while somewhat faster pulsars ($V_{z0} \sim 50 \text{ km s}^{-1}$) have periods ~ 100 Myr. By restricting our analysis to objects with $\tau_S < 10$ Myr, we can safely assume that our expressions above accurately account for vertical acceleration. For example, with $V_{z0} = 100 \text{ km s}^{-1}$ at 20 Myr, the Taylor series calculated velocity differs from the true current velocity by less than 3% despite changes of order 33%. Faster pulsars show smaller relative errors and slower ones, larger errors. (For initial z velocities of 20 km s^{-1} , the error is 4 km s^{-1} in the final z velocity.) Since our main purpose is to describe pulsar velocities statistically over the broad range of values encompassed by pulsars, this precision is more than sufficient. As a practical matter, errors in pulsar distances and the proper motions themselves dominate uncertainties in the approximations associated with the vertical motion.

The pulsar peculiar velocity (motion with respect to the mean disk in the vicinity of

²We assume the Sun is at midplane, even though there is evidence that it currently is ~ 15 pc above the plane (Hammersky *et al.* 1995).

the pulsar) is

$$\mathbf{V}^{(P)} = D\boldsymbol{\mu}^{(P)} + V_r^{(P)}\hat{\mathbf{n}} \quad (7)$$

where D is the distance, $\boldsymbol{\mu}^{(P)}$ is the peculiar proper motion and $V_r^{(P)}\hat{\mathbf{n}}$ is the line-of-sight peculiar radial velocity. The proper motion $\boldsymbol{\mu} = \boldsymbol{\mu}^{(P)} + \boldsymbol{\mu}^{(DGR)}$ where $\boldsymbol{\mu}^{(DGR)}$ is the known contribution from differential galactic rotation (DGR). The actual radial velocity is also composed of a peculiar part and a known contribution from DGR ($V_r = V_r^{(P)} + V_r^{(DGR)}$). The z-component of the peculiar velocity is

$$V_z^{(P)} = D\mu_W^{(P)} + V_r^{(P)} \sin b \quad (8)$$

and $V_z = V_z^{(P)}$ since the effects of rotation lie in the plane. One combination of the individually unmeasurable quantities $V_r^{(P)}$ and z_0 is determined in terms of the distance, current acceleration, peculiar proper motion and age (assumed known):

$$V_{r,eff} \equiv V_r^{(P)} + \frac{z_0}{t \sin b} = \frac{D}{t} + \frac{1}{\sin b} \left(\frac{\ddot{z}t}{2} - D\mu_W^{(P)} \right). \quad (9)$$

Note that $V_{r,eff}$ relates a particular combination of initial birth location and current peculiar radial velocity to directly measured quantities.

3.3. Likelihood Function for Radial Velocities & Birth Altitudes

We will use $V_{r,eff}$ to characterize individual objects: large values imply large peculiar radial motions and/or large initial birth heights. We seek the pdf of $V_{r,eff}$ given the uncertainties in the proper motion measurements and in the distance to individual objects. We treat this analysis as a preliminary attack on the determination of the 3D velocity distribution which is the subject of the following section.

We write the probability density function for the error in the proper motion measurement $f_{\delta\boldsymbol{\mu}}(\delta\boldsymbol{\mu})$ where the error is

$$\delta\boldsymbol{\mu} = \boldsymbol{\mu} - \tilde{\boldsymbol{\mu}} \quad (10)$$

and $\tilde{\boldsymbol{\mu}}$ is the reported value. We assume that the pdf for $\delta\boldsymbol{\mu}$ is a Gaussian with reported standard deviation $\sigma_{\boldsymbol{\mu}}$. For the distribution of $V_{r,eff}$ we are concerned with the component of proper motion out of the plane. Denote by $\overline{V_{r,eff}}$ the value of $V_{r,eff}$ when $\mu_W^{(P)} = \tilde{\mu}_W - \mu_W^{(DGR)}$ in Eq. 9 above. The pdf for an object with distance D , in direction $\hat{\mathbf{n}}$ and chronological age t is

$$\begin{aligned} f_{V_{r,eff}}(V_{r,eff} | \tilde{\mu}_W, D, \hat{\mathbf{n}}, t) &= \int d\delta\mu_W f_{\delta\mu_W}(\delta\mu_W) \delta(V_{r,eff} - \overline{V_{r,eff}} - [D\delta\mu_W / \sin b]) \\ &= \frac{\sin b}{D} f_{\delta\mu_W}(\mu_W^{(P)} + \mu_W^{(DGR)} - \tilde{\mu}_W). \end{aligned} \quad (11)$$

In the second line, $\mu_W^{(P)}$ is given explicitly by

$$\mu_W^{(P)} = \frac{\sin b}{t} + \frac{\ddot{z}t}{2D} - \frac{\sin b}{D}V_{r,eff}, \quad (12)$$

where $\mu_W^{(DGR)}$ and \ddot{z} are the position dependent differential galactic rotation contribution to the proper motion and the position dependent galactic acceleration. (For notational simplification, we suppress writing the direction and age in the pdf's that follow in this section.)

There is significant uncertainty in the distance to most pulsars. The pdf of $V_{r,eff}$ is expressed in terms of the range and distribution of distances allowed by observations. We have

$$f_{V_{r,eff}}(V_{r,eff} | \tilde{\mu}_W, D^*) = \int dD f_D(D) f_{V_{r,eff}}(V_{r,eff} | \tilde{\mu}_W, D) \quad (13)$$

where D^* stands for the imperfect distance knowledge and $f_D(D)$ is the corresponding pdf for distance. The specific form for the distance distribution may not be critical for all applications. If we are primarily looking for objects that are grossly discrepant with what we know about the disk scale height and the typical velocity of pulsars today, then a simple approximation may be sufficient. We assume a flat distribution for the distance in the interval $[D_L, D_U]$ where the lower and upper distance bounds are based on considerations of the TC distance model along with HI absorption and other measurements. In later sections, we will use an expression for $f_D(D)$ that is based on the expected number of pulsars in a population that would be visible.

The pdf has the form

$$f_{V_{r,eff}}(V_{r,eff} | \tilde{\mu}_W, D^*) = \frac{\sin b}{(D_U - D_L)} \int_{D_L}^{D_U} dD D^{-1} f_{\delta\mu_W}(\mu_W^{(P)} + \mu_W^{(DGR)} - \tilde{\mu}_W). \quad (14)$$

We use it to derive estimates for the covariant combination of the peculiar radial velocity and birth altitude of a given pulsar. The pdf determines the most likely value for $V_{r,eff}$ and associated confidence interval $[V_{r,eff}^-, V_{r,eff}^+]$. Then values for the peculiar radial velocity $V_r^{(P)}$ and birth height z_0 and individual confidence intervals may be found by using Eq. 9.

Initially, our analysis uses the chronological age $t = \tau_S$ for braking index $n = 3$ and no torque decay. Later in the paper, we consider alternative age estimates. To calculate the accelerations \ddot{z} in Eq. 12 we use a three-component model for the galactic potential (Paczynski 1990). To model differential galactic rotation, we use a flat rotation curve with circular velocity $v_{rot} = 220 \text{ km s}^{-1}$. Figure 2 shows $V_r^{(P)}$ plotted against $-0.5 \leq z_0 \leq 0.5$ kpc for all the pulsars in the sample. Also shown for three pulsars are dashed, parallel lines

that designate the 68% likelihood range in $V_r^{(P)}$ due to measurement errors in proper motion and to distance uncertainties. The figure demonstrates that, for most objects, solutions for $(V_r^{(P)}, z_0)$ exist with $z_0 \lesssim 0.3$ kpc and $|V_r^{(P)}| \lesssim 10^3$ km s⁻¹. Three objects (the Crab pulsar, B0540+23 & B0611+22) require $|z_0| \sim 0.2 - 0.3$ kpc within the plotted range of $V_r^{(P)}$. The allowed solutions imply that (1) the pulsar data are consistent with birth in the plane from Population I progenitor stars; and (2) no known pulsar younger than 10 Myr with a proper motion measurement need be born high above the galactic plane.

We also considered alternative relations between spindown and chronological ages. The braking index value $n = 2.5$ yields a roughly similar set of solutions but the situation becomes increasingly extreme as n decreases. For $n = 2$ some objects (e.g. 1933+16) have large $V_{r,eff}$, e.g. $|V_r^{(P)}| > 5000$ km s⁻¹ at $z_0 = 0$ kpc, or $|z_0| > 0.3$ kpc at $V_r^{(P)} = 0$ km s⁻¹. Figure 3 shows $(V_r^{(P)}, z_0)$ solutions for four pulsars for braking indices of 2, 2.5, 3 & 4.

4. THE 3D VELOCITY DISTRIBUTION

By combining the radial velocity constraints of §3 with proper motion measurements, it is possible to derive information on the full 3D velocities of pulsars and their birth distances from the galactic plane. Here we derive the joint pdf for birth z_0 and birth velocity.

We first relate the initial distribution function for pulsars at birth to the observed distribution function today. Then, we derive a likelihood function for proper motion data to be used to infer information about the initial peculiar velocity and birth height above the plane.

4.1. Birth & Present-day Distribution Functions

The distribution function for particles moving in a fixed background potential is related directly to the distribution function of initial conditions. Choose an inertial frame. At time t let the position be \mathbf{X} , the velocity \mathbf{V} and let the corresponding initial conditions be \mathbf{X}_0 and \mathbf{V}_0 . Liouville’s theorem states that the final and initial distribution functions satisfy $f_{\mathbf{X},\mathbf{V}}(\mathbf{X}, \mathbf{V}) = f_{\mathbf{X}_0,\mathbf{V}_0}(\mathbf{X}_0, \mathbf{V}_0)$.

We will apply this result to relate the initial and final pulsar distributions, bearing in mind that \mathbf{V}_0 is the sum of the circular rotation velocity and the peculiar motion, including the birth kick. The distribution of initial conditions $f_{\mathbf{X}_0,\mathbf{V}_0}(\mathbf{X}_0, \mathbf{V}_0)$ is expressed in terms of the initial peculiar velocity distribution $f_{\mathbf{X}_0,\mathbf{V}_0^{(P)}}(\mathbf{X}_0, \mathbf{V}_0^{(P)})$. If its age is sufficiently small, then the equations of motion show that the changes in peculiar velocity are small. To be

more precise, we ignore terms of $O(\Omega t, V_0^{(P)}t/R)$ compared to $V_0^{(P)}/v_{rot}$ where Ω is the circular frequency, R is the Galactocentric radius and v_{rot} is the rotation velocity. We also ignore variations with R , so we factor $f_{\mathbf{X}_0, \mathbf{V}_0} = f_{gp} \times f_{z, \mathbf{V}_0}(z, \mathbf{V}_0)$ into a constant two-dimensional, galactic plane part (f_{gp}) and a four-dimensional pdf in z and \mathbf{V}_0 . This is justified for particles (neutron stars) whose total radial displacement is small compared to the length scale for variations of disk properties. This approximation may be problematic given the maximum distances traveled in 10 Myr. The physical content of these assumptions is that the birth rate, birth scale height and initial velocity kick distribution do not vary appreciably over the range of the radial motion, at least for parts of the Galaxy that contribute to the observed pulsar sample. We find from Eqs. 7 and 8 that

$$z_0 = z - V_z t + \frac{1}{2} \ddot{z} t^2 = z - (D\mu_W^{(P)} + V_r^{(P)} \sin b)t + \frac{1}{2} \ddot{z} t^2 \quad (15)$$

$$\mathbf{V}_0^{(P)} = \mathbf{V}^{(P)} - \hat{\mathbf{z}} \ddot{z} t = (D\boldsymbol{\mu}^{(P)} + V_r^{(P)} \hat{\mathbf{n}}) - \hat{\mathbf{z}} \ddot{z} t. \quad (16)$$

The pdf of present-day pulsars is related to the pdf at birth by

$$f_{\mathbf{X}, \mathbf{V}}(\mathbf{X}, \mathbf{V}) = f_{\mathbf{X}_0, \mathbf{V}_0^{(P)}}(\mathbf{X}_0, \mathbf{V}_0^{(P)}) = f_{gp} f_{z_0, \mathbf{V}_0^{(P)}}(z_0, \mathbf{V}_0^{(P)}), \quad (17)$$

For convenience, we abbreviate $f_{z_0, \mathbf{V}_0^{(P)}}(z_0, \mathbf{V}_0^{(P)}) = f(z_0, \mathbf{V}_0^{(P)})$.

4.2. PDF of Proper Motion

Now we derive the likelihood function for the proper motion. We begin by forming the likelihood of a perfectly measured proper motion $\boldsymbol{\mu}$ for a pulsar with perfectly known position \mathbf{X} , displaced from the observer's position by $D\hat{\mathbf{n}}$. The pdf is

$$f_{\boldsymbol{\mu}}(\boldsymbol{\mu}|\mathbf{X}) = \frac{1}{\mathcal{N}_{\boldsymbol{\mu}|\mathbf{X}}} \int d^3\mathbf{V} f_{\mathbf{X}, \mathbf{V}}(\mathbf{X}, \mathbf{V}) \delta^2\left(\boldsymbol{\mu} - \frac{(\mathbf{V} - \mathbf{V}_\odot)_\perp}{D}\right). \quad (18)$$

Here $f_{\mathbf{X}, \mathbf{V}}(\mathbf{X}, \mathbf{V})$ is the present-day pulsar pdf; $\mathcal{N}_{\boldsymbol{\mu}|\mathbf{X}} \equiv \int d^3\mathbf{V} f_{\mathbf{X}, \mathbf{V}}(\mathbf{X}, \mathbf{V}) = f_{\mathbf{X}}(\mathbf{X})$ normalizes the proper-motion pdf; and \mathbf{V}_\odot is the velocity of the Sun due to galactic rotation.

The distribution of the *measured* proper motion $\tilde{\boldsymbol{\mu}}$, including measurement errors, is

$$f_{\tilde{\boldsymbol{\mu}}}(\tilde{\boldsymbol{\mu}}|\mathbf{X}) = \int d\boldsymbol{\mu} f(\tilde{\boldsymbol{\mu}}|\boldsymbol{\mu}) f_{\boldsymbol{\mu}}(\boldsymbol{\mu}|\mathbf{X}), \quad (19)$$

where $f(\tilde{\boldsymbol{\mu}}|\boldsymbol{\mu})$ is the likelihood of obtaining the measured value given the true one and is simply the usual Gaussian function for each component with standard deviations that reflect

measurement uncertainties. From our previous discussion, we assume $f(\tilde{\boldsymbol{\mu}}|\boldsymbol{\mu})$ depends only on the difference, $\delta\boldsymbol{\mu} \equiv \boldsymbol{\mu} - \tilde{\boldsymbol{\mu}}$, written as $f_{\delta\boldsymbol{\mu}}(\delta\boldsymbol{\mu})$. Let D^* stand for lower and upper cutoffs for D based on dispersion measure, known HII regions and so forth. Let $f_D(D|D^*, \hat{\mathbf{n}})$ be the resultant probability distribution. Marginalizing over the true distance,

$$f_{\tilde{\boldsymbol{\mu}}}(\tilde{\boldsymbol{\mu}}|D^*, \hat{\mathbf{n}}) = \int dD f_{\tilde{\boldsymbol{\mu}}}(\tilde{\boldsymbol{\mu}}|\mathbf{X}) f_D(D|D^*, \hat{\mathbf{n}}). \quad (20)$$

We can write the pdf for distances in the pulsar population described by $f_{\mathbf{X}, \mathbf{V}}$ assuming all such objects are visible. We find

$$f_D(D|D^*, \hat{\mathbf{n}}) = \frac{D^2 f_{\mathbf{X}}(\mathbf{X})}{\int dD D^2 f_{\mathbf{X}}(\mathbf{X})}, \quad (21)$$

where the integral is limited to the range implied by D^* . This is the point where we have ignored the detection-related aspects of the pulsar problem. Integrating over the perpendicular velocity we find

$$f_{\tilde{\boldsymbol{\mu}}}(\tilde{\boldsymbol{\mu}}|D^*, \hat{\mathbf{n}}) = \left[\mathcal{N}_{\boldsymbol{\mu}|D^*, \hat{\mathbf{n}}}^{-1} \int dD D^4 \int d\boldsymbol{\mu} \int dV_r f_{\delta\boldsymbol{\mu}}(\tilde{\boldsymbol{\mu}} - \boldsymbol{\mu}) f_{\mathbf{X}, \mathbf{V}}(\mathbf{X}, \mathbf{V}) \right]_{\mathbf{V}=\mathbf{V}_{\odot}+D\boldsymbol{\mu}+V_r\hat{\mathbf{n}}} \quad (22)$$

where V_r is the radial velocity in the inertial frame and $\mathcal{N}_{\boldsymbol{\mu}|D^*, \hat{\mathbf{n}}}^{-1}$ normalizes the pdf. To carry out the integrations ($d\boldsymbol{\mu}dV_r$) we change variables as follows: $\boldsymbol{\mu}^{(P)} = \boldsymbol{\mu} - \boldsymbol{\mu}^{(DGR)}(\hat{\mathbf{n}}, D)$ and $V_r^{(P)} = V_r - V_r^{(DGR)}(\hat{\mathbf{n}}, D)$ and use Eqs. 15-17 to give

$$f_{\tilde{\boldsymbol{\mu}}}(\tilde{\boldsymbol{\mu}}|D^*, \hat{\mathbf{n}}, t) = \mathcal{N}_{\boldsymbol{\mu}|D^*, \hat{\mathbf{n}}}^{-1} \int dD D^4 \int d\boldsymbol{\mu}^{(P)} \int dV_r^{(P)} f_{\delta\boldsymbol{\mu}}(\tilde{\boldsymbol{\mu}} - \boldsymbol{\mu}^{(P)} - \boldsymbol{\mu}^{(DGR)}) f(z_0, \mathbf{V}_0^{(P)}). \quad (23)$$

Note that $\boldsymbol{\mu}^{(P)}$ and $V_r^{(P)}$ are dummy integration variables and that the transformation to the initial peculiar velocity distribution requires knowledge of the chronological age. The data and the DGR contribution to the proper motion occur only in the pdf that describes the error distribution in the form of the difference: $\tilde{\boldsymbol{\mu}} - \boldsymbol{\mu}^{(DGR)}$. For cases of interest ($\tau_S \lesssim 10$ Myr), the acceleration correction to the velocity argument in Eq.16 is only a few tens of km s^{-1} and is, therefore, unimportant for establishing the velocity distribution of high-velocity objects. However, the correction to the spatial argument in Eq. 15 is significant. In the following, we ignore the velocity correction but apply the spatial correction.

4.3. Parameterization & Likelihood Function

The likelihood function for the parameters is the product over N_{psr} pulsars,

$$\mathcal{L} = \prod_{k=1}^{N_{psr}} \mathcal{L}_k, \quad (24)$$

where the likelihood factor, $\mathcal{L}_k \equiv f_{\tilde{\boldsymbol{\mu}}_k}(\tilde{\boldsymbol{\mu}}_k | \hat{\mathbf{n}}_k, D_k^*, t_k)$, for each pulsar is simply Eq. 23 evaluated using the measured proper motions (and errors) along with the distance constraints D_L, D_U , the direction $\hat{\mathbf{n}}$ and the age t .

To apply Eq. 23, we adopt a parametric approach, where we assume particular forms for the pdfs in z_0 and $\mathbf{V}_0^{(P)}$. Specifically, we assume that z_0 and $\mathbf{V}_0^{(P)}$ have a multicomponent Gaussian pdf of the form

$$f(z_0, \mathbf{V}_0^{(P)}) = \sum_{j=1}^{n_g} w_j g_{1d}(z_0, h_{zj}) g_{3d}(V_0^{(P)}, \sigma_{Vj}). \quad (25)$$

In Eq. 25, $g_{1d}(p, \sigma)$ is a standard 1D Gaussian pdf with zero mean and standard deviation σ , $g_{1d}(p, \sigma) = (2\pi\sigma^2)^{-1/2} \exp(-p^2/2\sigma^2)$, while g_{3d} is a 3D Gaussian $g_{3d}(q, \sigma) = (2\pi\sigma^2)^{-3/2} \exp(-q^2/2\sigma^2)$. The weights w_j sum to unity. The pdf is defined so that $fdz_0 d^3V_0^{(P)}$ is the infinitesimal probability.

We have chosen a multicomponent Gaussian model because its analytical properties allow it to fit a wide range of shapes for the actual distributions in z_0 and $\mathbf{V}^{(P)}$. There is not necessarily an implied *physical* basis for this choice of form: the different Gaussian velocity components need not correspond to different population components.

4.4. Results & Comparison of Models Using Odds Ratios

The parameters to be determined for a pulsar sample are (1) n_g standard deviations for velocities, σ_{Vj} ; (2) $n_h \leq n_g$ scale heights for the birth altitude, h_{zj} ; and (3) $n_g - 1$ weights, w_j for a total of $n_g + n_h - 1$ parameters.

We considered a set of models with increasingly complex velocity and birth height distributions. We label the models by $n_g.n_h$ and briefly describe them below:

1. [Model 1.1]: a single component model ($n_g = n_h = 1$)
2. [Model 2.1]: a two component velocity model with a single scale height ($n_g = 2, n_h = 1$)
3. [Model 2.2]: a model with two scale height and two velocity components ($n_g = 2, n_h = 2$) and
4. [Model 3.1]: a three component velocity model with a single scale height ($n_g = 3, n_h = 1$)

We assume flat priors for the parameters in selected ranges that are listed in Table 2. We generated the posterior probability distribution of parameters which is just the evaluation of the likelihood in the selected ranges. The modes of the posterior, i.e. the maximum likelihood results, and $\log \mathcal{L}$ appear in Table 3. These are the “best” values of parameters for each model. The analysis was repeated for several age cuts for the sample: $\tau_{Smax} = 1, 5 \text{ \& } 10$ Myr (for $n = 3$ and no torque decay). The mode of the distribution is typically well-defined. For example, in Figure 4 we display contours of $\log \mathcal{L}$ (log likelihood) for Model 1.1 with $\tau_{Smax} = 10$ Myr. The mode is identified by the cross. In Figure 5 we display contours for Model 2.1 in two-dimensional surfaces that pass through the mode.

The results in Table 3 clearly suggest the presence of a significant high velocity component when the models are sufficiently complex. At the same time, examination of the likelihood contours in the simplest model does not provide any obvious indications that its single 300 km s^{-1} component is inadequate. To make such a determination, we must compare the models in a systematic manner.

To compare models we use the odds ratio (cf. Gregory & Loredo 1992) to quantify goodness of fit while penalizing models with more parameters. We assume that all models are equally probable, *a priori*. The odds ratio reduces to the “Bayes factor,” which is the ratio of global likelihoods of two models (Gregory & Loredo’s Eq. 2.12). The global likelihood for a model M given data \mathcal{D} is

$$f(\mathcal{D}|M) = \int d\boldsymbol{\theta} f_{\boldsymbol{\theta}}(\boldsymbol{\theta}|M) \mathcal{L}(\boldsymbol{\theta}), \quad (26)$$

where $f_{\boldsymbol{\theta}}(\boldsymbol{\theta}|M)$ is the prior pdf for model parameters $\boldsymbol{\theta}$ and $\mathcal{L}(\boldsymbol{\theta})$ is the likelihood function as we have used it in this paper. We have already assumed the prior pdf is flat and we have seen that $\mathcal{L}(\boldsymbol{\theta})$ is strongly peaked. Thus, letting $\hat{\boldsymbol{\theta}}$ be the parameters that maximize $\mathcal{L}(\boldsymbol{\theta})$,

$$f(\mathcal{D}|M) \sim f_{\boldsymbol{\theta}}(\hat{\boldsymbol{\theta}}|M) \int d\boldsymbol{\theta} \mathcal{L}(\boldsymbol{\theta}) \equiv \frac{\Lambda_M}{V_M}, \quad (27)$$

where the last equation defines the integrated likelihood, $\Lambda_M \equiv \int d\boldsymbol{\theta} \mathcal{L}(\boldsymbol{\theta})$, and the volume in parameter space that is searched, $V_M = [f_{\boldsymbol{\theta}}(\hat{\boldsymbol{\theta}}|M)]^{-1}$.

We take the single Gaussian model with two parameters as our reference model: $M_1 \equiv 1.1$. The odds ratio for the M^{th} model relative to $M_{1.1}$ becomes

$$O_{M,M_1} \equiv \frac{f(\mathcal{D}|M)}{f(\mathcal{D}|M_1)} \equiv \frac{\Lambda_M}{\Lambda_{M_1}} \frac{V_{M_1}}{V_M}, \quad (28)$$

which we evaluate through numerical integration of the likelihood function for each model over a uniform grid in parameter space with bounds given in Table 2. The associated

volumes for the four models are:

$$\begin{aligned}
 V_{1.1} &= \Delta h_{z1} \Delta \sigma_{V1} \\
 V_{2.1} &= V_{1.1} \Delta w_1 \Delta \sigma_{V2} A_{2.1} \\
 V_{2.2} &= V_{1.1} \Delta w_1 \Delta \sigma_{V2} \Delta h_{z2} A_{2.2} \\
 V_{3.1} &= V_{1.1} \Delta w_1 \Delta w_2 \Delta \sigma_{V2} \Delta \sigma_{V3} A_{3.1}
 \end{aligned} \tag{29}$$

where $A_{2.1}, A_{2.2}$ and $A_{3.1} \leq 1$ are factors that account for the overlap in our search of parameter space for the maximum likelihood and the resulting degeneracy of the models.

The maximum likelihood values and the volumes yield the odds ratios given in Table 3. The odds ratios show that the data strongly favor the multiple-component models (models 2.1, 2.2 and 3.1) over the single-component model (1.1). However, the additional complexity of models 2.2 and 3.1 over 2.1 is not demanded by the data. This conclusion holds for the two largest age cutoffs considered (5 and 10 Myr). For a 1 Myr cutoff, the small number of data points appears to reduce the discriminating power between models and, consequently, we have ignored these results. The model fitting suggests that a single birth-z scale height of 0.13 kpc applies to both velocity components, which have rms velocities (3D) $\sim 175 \text{ km s}^{-1}$ and $\sim 700 \text{ km s}^{-1}$.

To refine the estimation, we derive the marginal distribution of each parameter. For a given parameter $\theta_j \in \boldsymbol{\theta}$, the marginal pdf is the normalized integral over all other parameters

$$f_{\theta_j}(\theta_j) = \frac{\int_{exc.\theta_j} d\boldsymbol{\theta} \mathcal{L}(\boldsymbol{\theta})}{\int d\boldsymbol{\theta} \mathcal{L}(\boldsymbol{\theta})}, \tag{30}$$

where the integral subscript ‘exc. θ_j ’ means that all parameters except the j^{th} one are integrated over. Fig 6 illustrates the marginal distributions for Model 2.1. Table 4 gives the best-fit values of parameters for the preferred Model 2.1 along with 68% confidence intervals. The confidence interval was calculated by finding the region in each marginalized distribution containing 68% of the area.

The mean 1D, 2D and 3D speeds are given by $\langle V_{1D} \rangle = \sqrt{2/\pi} \sum_j w_j \sigma_{Vj}$, $\langle V_{2D} \rangle = \sqrt{\pi/2} \sum_j w_j \sigma_{Vj}$, $\langle V_{3D} \rangle = \sqrt{8/\pi} \sum_j w_j \sigma_{Vj}$. For the best fit model (2.1), $\sum_j w_j \sigma_{Vj} \approx 264 \text{ km s}^{-1}$ and the three mean speeds are 211, 331 and 421 km s^{-1} . The speeds for the three-component Gaussian model (3.1) are nearly identical, while they are about 14% larger for the single-Gaussian model (1.1).

4.5. Spindown Ages & the Braking Index

The likelihood analysis we have presented is based on a braking index $n = 3$, an infinite torque decay time, τ_K (cf. Eq. 3), and a negligible birth period, P_0 . The analysis is sensitive to the spindown model because we infer the chronological age t from the spindown age τ_S . For example, Eq. 23 shows that the likelihood function depends on the initial distribution at z_0 and Eq. 15, in turn, shows that the birth position z_0 is a direct function of t as well as other observed (z) and marginalized ($V_r^{(P)}$, $\mu_W^{(P)}$) quantities. Here, we investigate how the results for the 3D velocity distribution depend on the braking index and decay time. As mentioned earlier, measured braking indices for very young pulsars (age $\sim 10^3$ to 10^4 yr) are less than 3, yielding spindown ages that are larger than we have assumed in our use of the conventional spindown age with $n = 3$. As n and τ_K are varied, ages for some objects increase while others decrease.

Figure 7 shows the log likelihood for the double Gaussian model (2.1) plotted against torque decay time, τ_K , for various values of braking index. *All* model parameters were varied to find the maximum likelihood. The likelihood peaks at $(n, \tau_K) \approx (2.5, 3 \text{ Myr})$ and the range of variation in the final likelihood value is small compared to that due to other model parameters. For example, the likelihood at $(n, \tau_K) = (3, 5 \text{ Myr})$ is only 22% smaller than the peak. If torque decay does not occur (i.e. $\tau_k \rightarrow \infty$), the peak likelihood is found at $n \approx 4.5$, but with a likelihood that is a factor 20.3 smaller than for $(n, \tau_K) \sim (2.5, 3 \text{ Myr})$. If torque decay is due to magnetic field decay with $n = 3$, the field decay time is twice the torque decay time, or $\sim 10 \text{ Myr}$.

The best values for the birth scale height, velocity parameters, and relative weights do not change appreciably with braking index and decay time. (It should be pointed out that we have used a fairly coarse grid in this analysis: $\Delta w_1 = 0.1$, $\Delta h_{z1} = 0.05 \text{ kpc}$, $\Delta \sigma_{V1} = 50 \text{ km s}^{-1}$ and $\Delta \sigma_{V2} = 200 \text{ km s}^{-1}$.) On the other hand, the mean sample age does vary in a easily characterized way. It is 2.95 Myr for $(n, \tau_K) = (3, \infty)$. For the best fit with $(n, \tau_K) = (2.5, 3 \text{ Myr})$ it is 1.64 Myr while the best fit with no torque decay for $n = 4.5$ yields 1.68 Myr. In the case with no torque decay, the best fit reduces all age estimates by the same factor, $3/4.5 = 0.67$. By contrast, for the absolute best fit for $(n, \tau_K) = (2.5, 3 \text{ Myr})$, some age estimates are increased while others are decreased.

Even though all model parameters were varied, the best parameter values for w_1, h_{z1}, σ_{V1} and σ_{V2} do not change significantly as the braking index and torque decay time are varied. Certain model parameters (e.g. σ_V) are directly tied to a measured quantity ($\mu^{(P)}$) and, hence, not susceptible to changes in t . Other model parameters (e.g. h_z) are strongly influenced by young objects at small $\sin b$ that have not had the opportunity to move far for any plausible ages. In addition, there are substantial errors in distance and

proper motion measurements and these overlay the intrinsic timescale change. Typical distance errors are factors of ~ 2 and typical proper motion errors are $\sim 50\%$. Thus it is not unreasonable that we distinguish spindown models that have typical age estimates that differ by ~ 2 .

The pulsar sample we have analyzed is more consistent with ages that are smaller, on average, than the conventional spindown ages. If no torque decay occurs, then “large” braking indices, $3 \lesssim n \lesssim 6$ are preferred over small braking indices, such as $n \sim 2.5$ measured for the Crab pulsar and $n \sim 2.4$ for B0540-69 in the LMC. If torque decay occurs, as is suggested by our best fit model, then a braking index of $2.5 - 3$ is preferred. An average braking index as small as 2 yields a likelihood that is $\sim 10^{2.9}$ times worse than the best fit model.

Our results are therefore at odds with those of Lyne *et al.* (1996), who estimate a braking index $n \sim 1.4 \pm 0.2$ for the Vela pulsar and who speculate that braking indices decrease as they age, at least in going from Crab-like pulsars ~ 1000 yr old to Vela-type pulsars about 20 times older. Lyne *et al.* conclude that pulsars are generally older than the conventional spindown age, in conflict with our conclusion.

Assuming the braking index for the youngest objects has been accurately determined, our results could be consistent with one of several proposed scenarios in which the braking index increased with age. Finite size corrections to the dipole spindown model (Melatos 1997) predict such an evolution. Heintzmann & Schruaffer (1982) noted that braking indices of older pulsars should be 3 or more based on plasma effects in the magnetosphere. Muslimov & Page (1996) suggested that, if the crustal magnetic field of neutron stars grows at early times (0.1 - 10 kyr), then braking indices should increase from $n < 1$ and asymptote to $n \rightarrow 3$ on a time scale of ~ 10 kyr.

In this analysis we have assumed that the birth spin period is much smaller than the present day period. There is evidence of discrepancies between spindown ages of some millisecond pulsars and ages constrained by temperatures of their white-dwarf companions (e.g. Camilo *et al.* 1994). Vivekenand & Narayan (1981) and Phinney (1996, private communication) have argued that pulsars may be born with nonnegligible spin periods (“injection”), in which case spindown ages overestimate chronological ages. The fact that the mean sample age of our most likely models is less than that of the magnetic dipole model without torque decay would be consistent with this suggestion. However, it does not follow that our analysis favors injection. In varying the spindown laws, the ages of all objects change, whereas if pulsars have a range of birth spin periods only objects with current periods comparable to birth periods have significantly altered ages. The set of spindown models we have tested does not cover the hypothesis of injection.

In §6 we explore the issue of pulsar ages in generality by deriving the distribution of chronological age for individual pulsars. This treatment starts from the kinematic data for each pulsar and our inferred scale height and velocity dispersion to deduce the age. The treatment is independent of the spindown model, *in so far as the scale height and velocity dispersion parameters are themselves insensitive to the precise form of the spindown model*, as appears to be the case. The general conclusion of the case-by-case analysis is consistent with the above conclusions: pulsars are on average roughly 50% younger than their conventional spindown ages.

5. 3D VELOCITIES OF INDIVIDUAL OBJECTS

In this section we use the global properties of the observed pulsar population (from §3) to aid estimation of the properties of individual pulsars. First, we write out a formal expression for the pdf for $\mathbf{V}^{(P)}$ and z_0 for an individual object given its distance limits, proper motion measurements, and the chronological age. In constructing the pdf, we incorporate as prior information the previously derived parameters for the distribution of birth altitude and velocity. Second, we Monte Carlo the resulting pdf to determine mean and mean square values for each pulsar in the sample. This highlights a number of interesting objects.

The analysis here is similar to the analysis of §3 but differs in that we estimate transverse speeds for each object and incorporate what we have learned from the 3D analysis of the whole population. The 3D velocities of individual objects can be used to test for correlations with other pulsar parameters.

Let Q be a quantity whose pdf we seek; Q may be a function of any of the observables, with functional form \tilde{Q} . Signify the data for a given pulsar as $\mathcal{D} \equiv \{D^*, \tilde{\boldsymbol{\mu}}, \hat{\mathbf{n}}\}$. For each object we estimate the chronological age t from P, \dot{P} and an assumed spindown model. Let \mathcal{I} represent the background information, including the posterior probability distribution for the model parameters governing the birth scale height, the velocity kick distribution and the relative weights of components. Since the posterior was found to be strongly peaked at the mode and the mode insensitive to the spindown model, we simply assume that \mathcal{I} sets the model parameters at the mode (i.e. the most likely values). We derive $f_Q(Q|\mathcal{D}, t, \mathcal{I})$ following the same general procedure used to derive Eq. 23. First, form the pdf for Q in terms of the distribution function for today's pulsar positions and velocities, assuming no observational errors in $\tilde{\boldsymbol{\mu}}$ and distance. Second, marginalize over the distance range and the proper motion errors. As before, we take Eq. 21 for the pdf for distance D between the upper and lower limits. Third, make the change of variables $d^3\mathbf{V} \rightarrow D^2 d\boldsymbol{\mu}^{(P)} dV_r^{(P)}$

and replace the present day pulsar distribution function with the corresponding initial distribution function. The result is

$$f_Q(Q|\mathcal{D}, t, \mathcal{I}) = \mathcal{N}_Q^{-1} \int dD D^4 \int d\boldsymbol{\mu}^{(P)} \int dV_r f_\delta \boldsymbol{\mu}(\tilde{\boldsymbol{\mu}} - \boldsymbol{\mu}^{(P)} - \boldsymbol{\mu}^{(DGR)}) f(z_0, \mathbf{V}_0^{(P)}) \delta(Q - \tilde{Q}) \quad (31)$$

where \mathcal{N}_Q^{-1} is the normalization constant; z_0 and $\mathbf{V}_0^{(P)}$ are the initial conditions (given by Eqs. 15 and 16); and the range of D integration is determined by D^* . The previously derived parameter values for birth scale height and peculiar velocity and the age occur in $f(z_0, \mathbf{V}_0^{(P)})$.

As a specific example of immediate interest, we take $Q = \{z_0, \mathbf{V}^{(P)}\}$ to give the joint pdf for the present day peculiar velocity and the birth altitude of an individual pulsar

$$f_{z_0, \mathbf{V}^{(P)}}(z_0, \mathbf{V}^{(P)}) \propto \left[D^2 f(z_0, \mathbf{V}_0^{(P)}) f_\delta \boldsymbol{\mu}(\tilde{\boldsymbol{\mu}} - \boldsymbol{\mu}^{(P)} - \boldsymbol{\mu}^{(DGR)}) \left| \frac{dD}{dz_0} \right| \right]_{D = \hat{D}} \quad (32)$$

$$\hat{D} = \frac{z_0 + \hat{\mathbf{z}} \cdot \mathbf{V}^{(P)} - \frac{1}{2} \ddot{z} t^2}{\sin b}.$$

The solution for \hat{D} is implicit because the vertical acceleration depends on D .

The expression clearly shows the role of the initial birth and velocity distribution $f(z_0, \mathbf{V}_0^{(P)})$ on limiting the allowed range of properties for a pulsar observed today. For poor or no observational constraints on proper motion, the birth distribution functions as a prior. However, if a proper motion measurement is precise, then $f_\delta \boldsymbol{\mu}$ provides a strong, perhaps dominant constraint on the velocity components and birth z for the object.

To apply Eq. 32 for each pulsar, we generate 200 Monte Carlo samples of z_0 and $\mathbf{V}^{(P)}$ using the method of rejection (cf. Rubinstein 1981; Press *et al.* 1992). For the pulsar age, we have assumed the canonical age given by Eq. 2 with $n = 3$ (i.e. magnetic dipole radiation and no torque decay). Table 5 gives the mean and rms values for $V \equiv \sqrt{V_r^{(P)2} + |\mathbf{V}_\perp^{(P)}|^2}$, $V_r^{(P)}$, $V_\perp^{(P)}$, and z_0 for the full sample. The two components for the perpendicular velocity ($V_{\perp 1}$, $V_{\perp 2}$) given in the table correspond to components in the right-ascension and declination directions. The rms values indicate the spread in possible solutions for each variable, subject to measurement errors in the proper motion, distance estimation errors and the fact that only two velocity components are determined by proper motion. Most objects show small average values for $V_r^{(P)}$, but with a large spread due to uncertainties in distance and proper motion. On the other hand, three objects require significant radial velocities, $V_r^{(P)} > 3\sigma_{V_r^{(P)}}$: B0943+10, B1953+50 and B2154+40. The latter two objects require radial velocity magnitudes ~ 1500 and ~ 1000 km s⁻¹, respectively. There are 8 objects with 3D mean velocity estimates exceeding 500 km s⁻¹: B1508+55, B1706-16,

B1842+14, B1933+16, B1946+35, B1953+50, B2154+40 and B2224+65. Of these, five have velocities in excess of 1000 km s^{-1} . Finally, 9 objects have birth z values that are determined to better than $3\sigma_{z_0}$: B0136+57, B0531+21 (Crab), B0540+23, B0611+22, B0630+17 (Geminga), B0656+14, B0740–28, B0833–45 (Vela), and B1929+10. Of these, three pulsars have $|z_0| \gtrsim 0.2 \text{ kpc}$. It is notable that these high z_0 pulsars are in the galactic anticenter.

6. PULSAR AGES

Now we derive the pdf for the chronological age, t , of a pulsar given its proper motion and distance measurements. Previously, we estimated t from the spindown time τ_S or its variants using alternative braking indices and torque decay times. Here, we rely solely on the kinematic information associated with each object and with the global parameters that characterize the birth scale height and initial peculiar velocity. These parameters were determined for a range of spindown models in §4.5 and the results were found to be only weakly dependent on braking index and torque decay time. This simplification means that the pdf for t is insensitive to the spindown assumptions made in the inferring the scale height and peculiar velocity parameters.

As we have previously emphasized, uncertainties in position and velocity are inextricably linked to the age uncertainty. We use Bayes' Theorem to relate the age pdf to the likelihood function for the data $\mathcal{D} = \{\tilde{\boldsymbol{\mu}}, \hat{\mathbf{n}}, D^*\}$:

$$f(t|\mathcal{D}, \mathcal{I})f(\mathcal{D}|\mathcal{I}) = f(\mathcal{D}|t, \mathcal{I})f(t|\mathcal{I}). \quad (33)$$

We assume that the prior probability for t , $f(t|\mathcal{I})$, is constant, consistent with a constant neutron-star birth rate over the recent past. We evaluate the likelihood of the data in the same manner as Eq. 23 to find

$$f_t(t) = f(t|\mathcal{D}, \mathcal{I}) = \mathcal{N}_t^{-1} \int dD D^4 \int d\boldsymbol{\mu}^{(P)} \int dV_r^{(P)} f(z_0, \mathbf{V}_0^{(P)}) f_{\delta\boldsymbol{\mu}}(\tilde{\boldsymbol{\mu}} - \boldsymbol{\mu}^{(P)} - \boldsymbol{\mu}^{(DGR)}) \quad (34)$$

where \mathcal{N}_t is the normalization constant.

Application to individual pulsars is straight forward. Figure 10 shows the pdfs $f_t(t)$ and corresponding cdfs for three pulsars. Also shown in the figure, as vertical lines, are the conventional spindown age estimates, τ_S . The shapes of the individual pdf's are directly related to the Gaussian shapes of the assumed underlying pdf's for z_0 , $\mathbf{V}_0^{(P)}$ and $\delta\boldsymbol{\mu}$. By inspection of Eq. 34, if measurement errors are infinitesimal and the values for birth z and D are fixed, then $f_t(t)$ has weight where $f(z_0, \mathbf{V}_0^{(P)})$ maximizes, in particular, near the

origin. If acceleration is not significant then the minimum $|\mathbf{V}_0^{(P)}|$ implies $V_r^{(P)} = 0$ and the minimum z_0 implies $t_0 \sim \sin b/\mu_W$. Thus, the maximum (or mode) of f_t is at an age t_0 . The figures show that the resultant pdf is not symmetric, falling off more slowly toward large t than small t because of the effect of peculiar radial velocity and the assumed Gaussian form: large $V_r^{(P)}$ (giving small t) has exponentially small probability of occurrence whereas small $V_r^{(P)}$ (giving large t) has only algebraically small probability.

Figure 11 shows the 68% probability ranges for the ages of the 47 pulsars in our sample along with the median, mode, and spindown age. As demonstrated in §4.5, our likelihood analysis shows a better fit to the pulsar data for combinations of braking index and torque decay time that make ages of most pulsars *smaller* than the conventional spindown age, $\tau_S = P/2\dot{P}$. The conventional spin down time assumes a braking index of 3, an infinite torque-decay time, and birth period much smaller than the present-day period. The same trend is apparent in Figure 11 which shows that the majority of objects have spindown ages $\tau_S > t_0$.

To further demonstrate that a bias exists between chronological and spindown ages, we inspect the ratio of chronological age to spindown age, $r = t/\tau_S$. The pdf for this ratio is

$$f_r(r) = \tau_S f_t(r\tau_S). \quad (35)$$

We average $f_r(r)$ over 45 objects in our sample, excluding the Crab and Vela pulsars because their kinematic ages are poorly constrained. Figure 12 shows the average f_r , which peaks at $r \sim 0.4$ and has a fast rise at smaller r and a slow decay for larger r . The mode of this pdf indicates that *kinematic ages are systematically smaller than conventional spindown ages*. This conclusion is in accord with our previous discussion, where we invoked specific mechanisms to maximize the likelihood in our velocity analysis and which also implied smaller kinematic ages. The results given in this section demonstrate this conclusion more directly and also show that it is a general trend in the population and not an artifact produced by a few extreme cases. Also, the pdf for age is calculated independently of any particular physical process, such as braking mechanisms other than that due to magnetic dipole radiation and torque decay.

7. CONSTRAINTS ON INDIVIDUAL PULSARS

In Appendix A we discuss constraints and uncertainties for particular objects, especially those with uncertain distances and large velocities. Here we comment on the possible birth sites and velocities of a few objects.

The Geminga pulsar (B0630+17) was discovered as a gamma-ray source and eluded

detection as a periodic source until 1992 (Halpern & Holt 1992). Recent parallax and earlier proper-motion observations (Caraveo 1993; Caraveo *et al.* 1996) yield fairly tight determinations of its distance and proper motion. Caraveo *et al.* discuss possible birth sites for this pulsar, including work by Gehrels & Chen (1993), Frisch (1993), Smith *et al.* (1994), and Cunha & Smith (1996). The latter three authors suggest birth in the event that has produced a supernova-like ring around λ Ori, a possible companion to the pulsar progenitor, now requiring a radial velocity of about -700 km s^{-1} . Our constraints on the radial velocity (Table 5), $V_r \approx 0 \pm 178 \text{ km s}^{-1}$ suggests this association is unlikely, essentially the same argument by Carveo *et al.*, who state that the velocity would make an unlikely small angle with the line of sight ($\sim 11^\circ$).

8. A VELOCITY-MAGNETIC MOMENT CORRELATION?

Various kick mechanisms suggest the magnetic field of a young pulsar is correlated with its acceleration.³ Horowitz and Piekarewicz (1996; see also Bisnovatyi-Kogan 1996) have discussed the role of parity violation for neutrinos interacting with electrons and nucleons in a strong magnetic field. Several interactions (neutrino scattering from polarized nucleons, from polarized electrons, and in the presence of a polarized background of electrons) can couple the momentum flux of the neutrinos to the B field direction with a magnitude proportional to B, potentially leading to the recoil of the entire neutron star. A field of $\sim 10^{16} \text{ G}$ is needed to achieve the observed velocities. A more speculative suggestion of Kusenko & Segrè (1996a) is that neutrino oscillations are effected by the strength of the magnetic field. If the field is sufficiently strong ($\sim 10^{14} \text{ G}$ according to the original proposal, $\sim 10^{16} \text{ G}$ according to revised estimates by Qian 1997), then interconversion of ν_e and ν_τ between the two different neutrinospheres allows some of the trapped electron neutrinos to convert to the tau form and escape. Neutron star recoil results from anisotropic emission of neutrinos and the resultant momentum impulse. The resonant interconversion depends on the function $\hat{k} \cdot \vec{B}$ and the *net* momentum impulse could vanish for certain perfectly symmetric field configurations (e.g. a strong, exactly toroidal field but not a dipole field). Kusenko & Segrè (1996b) discussed an expected correlation in their model, $v \propto B$ for long

³According to the “rocket theory” of Harrison & Tademaru (1975), pulsars with off-axis magnetic dipoles are accelerated as they spin down. For rapidly spinning neutron stars, the final velocity is independent of the magnetic moment since larger magnetic moments cause a larger force that acts for a shorter time. The net velocity created by the Harrison-Tademaru rocket depends on the birth period and offset of the magnetic axis and one would not expect to find a correlation between a pulsar’s velocity today and its initial magnetic field. However, a relation between the offset and magnetic field strength would introduce a correlation.

period pulsars. Birkel and Toldrà (1997) considered the correlation between transverse velocity and the estimated magnetic field projected along the pulsar spin axis for short period objects. The former find evidence in favor of the hypothesis, the latter do not.

Some previous investigations have identified significant correlations between perpendicular velocities and magnetic moment (e.g. Anderson & Lyne 1983; Cordes 1986, 1987; Bailes 1989) to varying degree and others have not (Lorimer, Lyne & Anderson 1995). Using the derived velocities for our sample, we tested for a correlation between the 3D velocities of Table 5 and various combinations of P and \dot{P} by cross correlating $\log V$ and $\log P\dot{P}^\beta$. Figure 13 shows the correlation coefficient plotted against β . The correlation maximizes at $\beta = 0$ with a correlation coefficient of 0.26, which can be achieved by chance at the 7.8% level. This indicates that the 3D velocity is not correlated with the magnetic moment ($\beta = 1$) or with the spindown age ($\beta = -1$) or any other combination that involves a significant contribution from \dot{P} . Moreover, velocities are at most weakly correlated with spin period.

Since there has been some disagreement over the significance of the correlation in the past, we provide the following discussion. The previously analyzed samples included objects which have been spun up, i.e. millisecond pulsars, and which have significantly lower space velocities and smaller magnetic fields than the young, pulsars considered in this paper. As shown in paper I, (Cordes & Chernoff 1997) the nominal rms 3D velocity for MSPs $\sim 80 \text{ km s}^{-1}$ is a factor ~ 5 smaller than that of young pulsars. It seems clear that the correlations between V and $P\dot{P}$ previously identified were effectively measuring this difference between the young and MSP populations. As argued in paper I, both the low magnetic fields and space velocities of MSPs are related to the required binary configuration needed in order for accretion driven spinup to occur. Accretion quenches or rearranges the magnetic field of the pulsar so as to diminish its apparent dipolar magnetic field. Binaries that are not disrupted have low center of mass velocities. This economical interpretation suggests that the apparent V - $P\dot{P}$ correlation has nothing to do with the physics of core collapse that produces neutron stars. Bailes (1989) has suggested one scenario where a pair of NSs are created from a binary. The binary evolves in such a way to produce one strong-field, high-velocity NS and one low-field, low-velocity NS. Our interpretation and our statistical results on the kinematics of pulsars are consistent with this scenario but do not require the particular assumptions of his model.

Although we find no evidence of correlation between v and B , we do not regard that as particularly strong evidence for or against the role of neutrino-mediated parity violations or neutrino oscillations. The magnetic field required for these schemes is $\sim 10^{14} - 10^{16} \text{ G}$, much larger than the inferred dipolar field today. Thus, the original field must have decayed

by $10^2 - 10^4$ and it is unclear what relationship today’s residual field bears to the field that acted during the epoch of acceleration.

9. PULSAR-SUPERNOVA REMNANT ASSOCIATIONS

Frail, Goss & Whiteoak (1994) deduce a mean transverse velocity $\sim 550 \text{ km s}^{-1}$ for 12 pulsars near supernova remnants, using the apparent angular offset between pulsar and remnant centroid, a distance estimate, and an age estimate, taken to be the conventional spindown age. One association in their sample (B1757 – 24 & G5.4 – 1.2) yields a transverse speed $\sim 1800 \text{ km s}^{-1}$. A few others were excluded on the basis of their ‘extreme’ velocities, ranging from 1600 to 3600 km s^{-1} , including an association between PSR B1610 – 50 and Kes 32 proposed by Caraveo (1993).

Our constraints on kinematic pulsar ages (§6) are based on objects that are much older than the characteristic 20 kyr age of those in the Frail *et al.* sample. If there is no field decay, the most likely braking index, $n \approx 4.5$, implies that the Frail *et al.* velocities are biased too low by about a factor of two. The mean transverse speed in the Frail *et al.* sample would then be $\sim 1100 \text{ km s}^{-1}$, which is about 3 times higher than the mean transverse speed in our best-fit model 2.1. If there is field decay on a timescale of 3 Myr and a braking index $n \approx 2.5$ (as in our best model), then the Frail *et al.* sample will have ages that are slightly *larger* than the conventional spindown times by a factor $3/2.5 = 1.2$, thus reducing the mean, transverse velocity in Frail *et al.* by about 20% to $\sim 460 \text{ km s}^{-1}$, which is still larger than the transverse mean ($\sim 331 \text{ km s}^{-1}$) of our velocity distribution by 26%.

In either case, the velocities calculated from pulsar-supernova remnant associations are larger than the mean pulsar distribution. This is intriguing and may indicate that supernova remnants are produced preferentially by the explosions that yield fast kicks. It is clear that a statistical analysis of the significance of the pulsar-supernova remnant associations and a more complete analysis of the selection effects in the pulsar surveys are needed. For example, some of the higher velocity objects in the Frail *et al.* sample may be spurious associations. To gain some sense of the incompleteness of the pulsar survey at high velocity, we can assume that the 12 associations used by Frail *et al.* are real and estimate a correction to the pulsar birth rate for the selection against high-velocity objects in pulsar surveys as follows. Frail *et al.* estimate a median velocity $\sim 460 \text{ km s}^{-1}$ that we correct to 380 km s^{-1} (using a braking index of 2.5). From our velocity pdf based on 47 pulsars with average spindown age 2.95 Myr, we find $P\{V_{\perp} > 380 \text{ km s}^{-1}\} = 0.22$. Assuming identical low velocity distributions, our sample is depleted of high velocity pulsars by a factor $0.5/0.22 \sim 2.3$. For all velocities the sample has been depleted by a factor $1/0.72 \sim 1.4$.

Thus, if the Frail *et al.* estimates are correct, then about 40% of pulsars are missed due to selection against high-velocities.

10. ASTROPHYSICAL CONSEQUENCES

In this section we discuss a few of the astrophysical implications of the results we have reached.

10.1. Evidence for Asymmetric Supernova Kicks

The large peculiar velocities we have estimated for pulsars—and their distribution—are the net result of kicks from supernova explosions, including rocket-like accelerations (Harrison & Tademura 1975), and disrupted orbital motion in those cases where a neutron star, or its progenitor, have become unbound from a binary or multiple star system.

A considerable body of evidence supports the conclusion that supernova explosions are, in general, asymmetric so as to impart significant velocities to neutron stars. This evidence includes (1) statistical arguments based on population synthesis studies which indicate that symmetric explosions yield too many binary radio pulsars and too small a mean speed (Dewey & Cordes 1987; hereafter DC87); (2) the existence of objects, like the Guitar Nebula pulsar (B2224+65), which have velocities larger than that of any plausible progenitor binary; (3) the occurrence of geodetic precession in two NS-NS binaries, which requires a misalignment of the spin and orbital angular momenta through explosion asymmetry (Cordes & Wasserman 1984; Weisberg *et al.* 1989; Cordes, Wasserman & Blaskiewicz 1990; Arzoumanian *et al.* 1996) suggestive of a kick $\sim 100 - 300 \text{ km s}^{-1}$; (4) orbital precession in the pulsar J0045-7319, probably the result of spin-orbit coupling (Lai *et al.* 1995; Kaspi *et al.* 1996). Assuming aligned angular momenta in the pre-supernova state, Kaspi *et al.* infer a probable minimum kick of 100 km s^{-1} to achieve the current misalignment of spin and orbital momenta.

Quantitatively, except for the Guitar nebula pulsar, these facts each call for kicks $\gtrsim 100 \text{ km s}^{-1}$. For example, DC87 concluded that $\sim 90 \text{ km s}^{-1}$ kicks were needed to account for the then-observed $\sim 100 \text{ km s}^{-1}$ pulsar velocity distribution and the low binary frequency of pulsars. Current population synthesis models of neutron star containing binaries predict birth rates of wide and close radio pulsar binaries and of high mass X ray binaries in rough agreement with observations when kicks are drawn from a Gaussian with dispersion $\sim 450 \text{ km s}^{-1}$ (Portegies Zwart & Verbunt 1996). Without the kick, far too

many Be-pulsar binaries, Be- and high-mass X-ray binaries and binary radio pulsars are found. It is important to note that the minimum kick needed to remove the wide binaries is less than that needed to explain the proper motions studied in this paper. Also, the only direct measurement of very fast $\sim 1000 \text{ km s}^{-1}$ objects is that of the Guitar nebula pulsar. Indirect evidence comes from statistical studies of proper motion like the current one and that of Lyne & Lorimer (1994). Less clear evidence comes from associations of pulsars with some supernova remnants of known age (see §9).

10.2. High Velocities and Escape from the Galaxy

The current results extend previous results in a number of ways. We begin with the high velocity end of the pdf. The pulsar sample itself includes 5 examples (11 %) whose inferred 3D velocities exceed 1000 km s^{-1} .

Our model fitting allows us to estimate the fraction of objects that have sufficient total velocity to escape the Galaxy. The escape velocity is, of course, not known with precision and it is a strong function of location in the Galaxy. Leonard & Tremaine (1990) place a lower bound on the local V_e of 430 km s^{-1} . Integrations of the Paczynski potential also indicate that 500 km s^{-1} is a representative estimate for V_e , so we take this as a fiducial value.

In Figure 8 we show the pdfs for the peculiar speed and the cumulative distribution functions (cdfs) of speed for three models ($n_g \cdot n_h = 1.1, 2.1$ & 3.1). The poorly-fitting, single-component model (1.1) suggests that 50% of the known, young pulsars will escape the Galaxy. The best model (2.1) and slightly-worse model (3.1) yield a more modest $\sim 20\%$. The cdf for pulsar speeds indicates 5-25 % above 1000 km s^{-1} , taking into account uncertainties in our fitting, as indicated in Figure 8.

In interpreting these results, it is necessary to reiterate that the pulsar sample is known to be strongly biased by selection effects, many of which arise from the fact that pulsar surveys are signal-to-noise limited. Many factors contribute to the net S/N for a given pulsar, including period dependence of the underlying pulsar beam shapes and luminosity. More importantly, however, is the velocity selection that occurs (Helfand & Tadamaru 1977; Cordes 1986; Lorimer & Lyne 1994): a greater number of fast pulsars will move out of the detection volume centered on the Earth than will move into it. Thus, pulsar surveys are biased against high velocity pulsars. The magnitude of this bias depends on details of specific pulsar surveys. Our analysis does not incorporate the detection-related part of the observer’s selection function (see introduction) and it is not possible to correct *post facto*

the derived pdf. We are currently working on incorporating the detection-related terms to the selection function (Chernoff & Cordes 1997). The velocity pdf derived by Lyne & Lorimer (1994) has an overall shape that is similar to our double Gaussian model, but predicts a larger fraction of pulsars that will escape the Galaxy, $> 50\%$.

10.3. Number of Separate Velocity Components

The two component distribution, Model 2.1, we have found to be the best fit in §4.4, may or may not correspond to two physical subcomponents in the Galactic population of radio pulsars. Our original assumption was that the sum-of-Gaussians form would suffice to model any actual pdf, with no implication that the individual Gaussians corresponded to distinct physical subpopulations. However, the fact that the three component model has an odds ratio inferior to the two component model and, in addition, that there is a significant disparity between the individual velocity parameters ($\sigma_{V1} \sim 4\sigma_{V2}$) is suggestive that two distinct subpopulations may be involved. At the same time, we note that we have explored only Gaussian models and that testing other parametric forms will be necessary before drawing this conclusion.

To test for the presence of an additional low-velocity population of pulsars, we explored solutions where two of the components were varied near our best fit for the two-component model (2.1) and a third additional component was imposed with dispersions in the range $10 \text{ km s}^{-1} \leq \sigma_{V3} \leq 210 \text{ km s}^{-1}$. By varying the weights, w_1, w_2 , dispersions σ_{V1}, σ_{V2} while holding the birth scale height (h_{z1}) fixed, we find $w_3 \leq 0.02, 0.05, 0.1$ for $\sigma_{V3} \leq 30, 50$ and 70 km s^{-1} , respectively. We therefore find no evidence in the data for a low-velocity component that might provide a signature of symmetric supernovae in isolated pulsars or in wide binaries. There is only a few percent allowed for pulsars with speeds less than 50 km s^{-1} , consistent with the appearance of only two objects in our sample (B1747–28 and B1929+10) whose 3D speeds could be, but need not be, this small.

If there were no intrinsic kick then isolated supernovae would produce low velocity neutron stars with velocities of order their progenitors' speeds, $\sim 30 \text{ km s}^{-1}$. The fraction of NS that originate from isolated (nonbinary) progenitors is not well known. In the models of Portegies Zwart & Verbunt (1996) composed of 40% single stars, 60% binaries, with LL type kicks at birth (models SS and AK) approximately 34% of all supernova occur in isolated progenitors, 66% in binaries. Since our model implies that there are relatively few low velocity pulsars, a natural interpretation is that all neutron stars receive a substantial kick at birth.

This conclusion is at variance with the recent proposal of Iben and Tutukov (1996) that there are no intrinsic kicks during supernova collapse, that instead, the pulsar velocity is produced entirely by the breakup of binaries. To avoid overproducing low velocity pulsars, Iben and Tutukov posit that pulsars can arise only from stars in which mass transfer or tidal interactions function to spin up the star prior to collapse. Comparison with the Portegies Zwart & Verbunt results shows that this assumption is not sufficient to zero out the low velocity part of the pdf. Roughly half of the supernovae in binaries involve mergers of stars prior to the explosion. We anticipate that the merged objects will resemble single stars in their center of mass motion but will contain substantial spin angular momentum. If these objects form neutron stars as the population synthesis models predict and if the neutron stars become visible pulsars but do not receive birth kicks then they will contribute weight to the low velocity part of the pdf. This is not what we observe. Thus, whether or not single stars give rise to pulsars it appears that kicks $\gtrsim 50 \text{ km s}^{-1}$ are *generally required* for consistency with the pdf.

A supernova kick of $\sim 100 \text{ km s}^{-1}$ has generally been called for in population synthesis models (DC87): otherwise too many neutron star containing binaries are created. It is satisfying that the binary abundance gives results consistent with the low velocity end of the pulsar pdf. These abundances are an intrinsically less clear cut constraint because of the many complexities of binary evolution including the uncertainties implicit in the initial conditions. On the other hand, the small size of our current sample limits the precision of the direct determination of the pdf at low velocity. Future proper motion measurements should improve the situation.

Recent searches for old, accreting, isolated neutron stars have turned up few prospects (see Wang 1996 for a review and Manning, Jeffries & Willmore 1996 for limits on the ROSAT Wide Field Camera survey). Our results imply that fewer than 10% of neutron stars move with velocities less than 70 km s^{-1} (see above). This differs from the estimates of $\sim 25 - 30\%$ used by Madau & Blaes (1994) which were based on the young pulsar velocity distribution of Narayan & Ostriker (1990), diffusively heated by gravitational interactions. Since Bondi-Hoyle accretion scales as v^{-3} , the new velocity distribution should play an important role in determining the number of detected objects in X ray surveys and may help reconcile the paucity of sources and the theoretical predictions. The accretion rate onto the star depends also on the strength of the magnetic field and the rotation rate, so our estimates of the braking index and torque decay timescale are relevant too.

For supernovae in binaries that do not involve mergers (roughly 30%) the resultant velocity distribution represents a convolution of the orbital velocity distribution with the intrinsic kick velocity distribution. The maximum velocity attainable with 90 km s^{-1}

kicks for initial masses up to $20M_{\odot}$ was estimated by DC87 to be about 600 km s^{-1} (by reaction [N1], with such a small separation that the supernova shock completely destroys the companion) but this constituted $< 0.2\%$ of all formed neutron stars. A more significant 8% contribution of $\sim 500 \text{ km s}^{-1}$ was found in reaction [N3] in which non-conservative evolution creates an unbound neutron star and white dwarf. These numbers are, of course, only examples based on the input quantities used by DC87; especially important is their attribution of final (pre-explosion) orbital periods after the spiral-in processes that influence the N1 and N3 paths; these periods were only guessed at, implying that the typical 500-600 km s^{-1} velocities estimated for these paths are not hard numbers.

Iben and Tutukov (1996) argued that the highest orbital velocity of neutron star are created when the primary-descended neutron star in a binary is released as a consequence of a second supernova explosion. They envision a semi-detached binary consisting of a $16M_{\odot}$ He core and an neutron star with a $1.7R_{\odot}$ semi-major axis. The orbital velocity is $\sim 1300 \text{ km s}^{-1}$ and the first neutron star is ejected at $\sim 900 \text{ km s}^{-1}$. Given that the initial mass of the main sequence progenitor of the He core is about $40M_{\odot}$, close to the maximum mass for a star to yield a neutron star, their example provides an upper bound to the possible orbital velocity. Our result that 5 of the pulsars have velocities in excess of 1000 km s^{-1} then provides decisive evidence that kicks of some sort are required.

In the future, once the observational selection effects are more fully accounted for, it will be important to analyze the velocity pdf in detail. At the moment, we make a few general comments. An outstanding issue is whether the two Gaussian description corresponds to a single distribution with an extended high velocity tail or whether it more closely corresponds to two separate populations of pulsars. Our two component results imply low and high velocity pulsars with comparable numerical weights (based on the crude estimate of the selection against high velocity pulsars above). If the contribution from the kick and from the orbital disruption of binaries were randomly combined (in the sense of two random velocities drawn from individual Gaussians) then the resulting distribution would be unimodal in speed with a dispersion that is the root mean square of the individual dispersions. The current result is not unimodal.

This may be an indication that the two known velocity sources, orbital motion and intrinsic supernova kick size, are correlated. For example, binaries in which super giants explode will generally be larger than those in which He cores explode (since mass transfer has occurred in the second but not the first case). If the kick size of the former is smaller than the latter, then the pdf for velocity may have two distinct components. In fact, supernovae will occur in a variety of modified stellar types in binaries (He core, CO core, Wolf-Rayet and super giant according to Portegies Zwart & Verbunt 1996) and more

complicated correlations with orbital motion can be expected. Another possibility is that the merged stars with no orbital motion but large angular momentum may experience kicks of a different characteristic size than regular or stripped stars. While all these possibilities are speculative, the accurate determination of the pdf, whether or not it is unimodal, promises to be of value in elucidating the complexities of binary evolution.

10.4. Implications for core collapse

An important aspect of this work is that we establish that a significant fraction of the pulsar velocity distribution lies above 1000 km s^{-1} . This should provide important constraints on numerical simulations of supernova explosions.

In a supernova collapse the energy scales are 10^{53} ergs for neutrino emission and neutron star binding energy, 10^{51} ergs for mass motions plus optical display, and 1.4×10^{49} ergs for a 1.4 solar mass neutron star moving at 1000 km s^{-1} . Thus, the energy involved in NS motion is but a small fraction of the total. Moreover, the NS velocity is quite small relative to free fall velocities in the vicinity of the core. It is interesting to note that the distance traveled by the core moving at a typical speed of 1000 km s^{-1} for an interval corresponding to the delay before explosion (0.07-0.42 s for SN1987a as estimated by Bethe 1993) is substantial compared to the characteristic dimensions of the system. Bethe estimates three important lengthscales: the neutrinosphere where the optical depth to neutrinos becomes of order unity (20 km), the gain radius where heating by the radiated neutrinos exceeds the gas' cooling ($\sim 140 \text{ km}$) and the free nucleon radius where alpha particles are completely dissociated into neutrons and protons ($\sim 210 \text{ km}$). As the protoneutron star forms, the accretion shock stands off at $\sim 300 \text{ km}$ and begins to accelerate outward once the ram pressure of the accreting material diminishes sufficiently. The neutrino heating and convection behind the shock are essential for providing the pressure that launches the shock. The core's motion is slow and the material between the neutron star and the shock is subsonic, so whatever acceleration mechanism functions, it should make little difference for estimating the state of the normal matter within the shock.

We begin by describing the limits to the generation of core motion. If the kick Δv_{ns} is ultimately due to the momentum impulse associated with anisotropic neutrino emission, then a firm limit may be expressed in terms of the total binding energy of the neutron star, e.g.

$$\Delta v_{ns} < \epsilon_\nu \frac{\Delta E}{M_{ns} c^2} c \quad (36)$$

where ϵ_ν is the anisotropy in the neutrino momentum and ΔE is the total energy emitted,

which must be less than the binding energy of the final neutron star $\approx 0.15M_{ns}c^2$. To give kicks of 1500 km s^{-1} , we require that $\epsilon_\nu > 0.03$. From numerical simulations, Janka & Müller estimate that the energy that is available is significantly less than the binding energy – more closely the accretion of the mantle during the convective period: $\Delta E \approx 0.015M_{ns}c^2$. Then a substantially larger asymmetry $\epsilon_\nu > 0.3$ is required to give 1500 km s^{-1} . This degree of asymmetry is inconsistent with simulations.

If the kick is due to the momentum recoil from either accreted or expelled matter, the momentum transfer is of order the escape velocity near the gain radius times the mass contained between the gain region and the accretion shock front times an asymmetry factor, e.g.

$$\Delta v_{ns} < \epsilon_{ej} \frac{\Delta M}{M_{ns}} v_{ej} \quad (37)$$

where ϵ_{ej} is the anisotropy in the momentum carried off, ΔM is the mass and v_{ej} is the escape velocity. From numerical simulations, Janka & Müller estimate from the most extreme cases that $\Delta M/M_{ns} < 0.2$, $v_{ej} < 0.1c$ and $\epsilon_{ej} < 0.08$ and infer $\Delta v_{ns} < 500 \text{ km s}^{-1}$. Once again, a substantially larger asymmetry $\epsilon_{ej} > 0.24$ would be required to give 1500 km s^{-1} .

These general arguments are not without loopholes, of course. They depend on the validity of the existing numerical simulations to set reasonable limits for ϵ_ν or ϵ_{ej} . In all calculations to date the neutron star is fixed at the center of symmetry. As mentioned above, because the fastest neutron star motions are subsonic these approximations should be reasonable for gauging the size of purely hydrodynamic quantities like ΔM , ΔE , v_{ej} and ϵ_{ej} that appear above. The fact that neutrino transport is treated with limited accuracy and that current numerical modeling is not done in full 3D are much more difficult issues to evaluate.

As many others have discussed, it would appear that the likely physical sources for a kick are (1) the large neutrino flux beyond the neutrinosphere and (2) the outer envelope of infalling material which is not in sonic communication with the matter surrounding the core. Goldreich, Lai & Sahriling (1997) have suggested that core g modes in presupernova stars may be overstable. As the matter collapses, irregularities in the infalling envelope may grow to large amplitude and ultimately impart a kick by gravitational torques. Another possibility is envisioned by Burrows and Hayes (1996) in which the inhomogeneities of the infalling matter channel the supernova blast into a jet-like outflow that causes the core to recoil.

It is important to point out, also, that the lack of correlation between the velocity and magnetic field in today’s pulsars (§8) does not necessarily rule out a neutrino-magnetic field

interaction ultimately responsible for the recoil. If field decay has occurred, as suggested by our best fitting models with torque decay, then the correlation between magnetic field and velocity could be weakened.

11. SEARCHING FOR THE HIGHEST-VELOCITY PULSARS

It is almost certain that the velocity pdf we have derived underestimates the fraction of pulsars with $V \gtrsim 10^3 \text{ km s}^{-1}$. Searching for high velocity pulsars at high galactic latitudes is a clear, though nontrivial, way to improve the situation. The difficulty arises because (1) such pulsars will be faint owing to their presumably large distances; (2) proper motion measurements will require VLBI techniques; given pulsar faintness, the VLBA will have to be augmented by the large-aperture Arecibo Telescope and Green Bank Telescope; (3) high-velocity pulsars will be above the thickest free electron layer in the Galaxy and therefore their distances cannot be estimated from the TC (or any other) model for the electron density. Difficulties (1) and (2) can be surmounted through suitable allotment of telescope time. Estimating pulsar distances is much more difficult to tackle, for inverting dispersion measures will never be possible for pulsars with $|z| \gtrsim 1 \text{ kpc}$. Parallax observations with VLBI or pulse-timing techniques are also unlikely. The only possible recourse is development of an alternative distance scale. We are investigating the possibility that radio pulsars have beam components whose luminosities are determined by P and \dot{P} and no other parameters. This ‘standard candle’ approach also requires that beam shapes and angular diameters also be predictable, in which case orientation angles between the pulsar spin and magnetic axes and the observer’s direction can be determined, along with the predicted flux and, hence, distance. Work on this beam modeling will be reported elsewhere. Should beam modeling fail due to (e.g.) pulsar ‘weather’ effects, such as severe distortions of magnetic fields from dipolar forms by accretion or other history dependent activity, then analysis of high latitude pulsars must rely on statistics of large numbers of objects rather than velocity estimates of individual objects.

12. SUMMARY AND CONCLUSIONS

In this paper we have used the data on 47 pulsars to infer their velocity and z-altitude distributions at birth. Our likelihood method allows estimation of radial as well as transverse velocities, contingent on estimates for the ages and birth z’s of individual objects. We emphasize that we have not corrected the results for the strong selection effects in the original pulsar surveys that have provided the sample of objects. The strongest effect on

our conclusions is that we have underestimated the fraction of pulsars with large velocities, e.g. those with $V > 1000 \text{ km s}^{-1}$. We are currently developing methods, similar to those in this paper and in Paper I, that take selection effects into account.

With these provisos, we have found that:

1. All pulsars in the sample are consistent with birth within 0.3 kpc of the galactic plane; any apparent motion of pulsars toward the galactic plane is easily explainable as a combination of projection effects associated with pulsars that are relatively nearby, a conclusion made long ago, on a smaller sample, by Helfand & Tademaru (1977).
2. The best fit model we have found consists of two Gaussian components in velocity, with dispersions ~ 175 and 700 km s^{-1} , combined with a birth scale height of 0.13 kpc; we have not investigated mathematical forms other than the multicomponent Gaussians.
3. With our fit, we predict that $\sim 20\%$ of pulsars like those in our sample will escape the Galaxy; a rough estimate indicates that this fraction may be underestimated by a factor ~ 2 due to selection effects.
4. A braking index $n \sim 2.5$ is favored if the pulsar torque constant decays on a time scale $\sim 3 \text{ Myr}$. If no torque decay occurs, then most braking indices are in the range 3.5-6, though such a model yields a slightly inferior likelihood than does the model with torque decay.
5. The constraints on braking index and torque decay time arise from the role that the kinematic age plays in our estimates of radial velocities. The most general statement is that pulsar ages are typically a factor ~ 2 smaller than the conventional spindown ages calculated as $P/2\dot{P}$, which assumes birth at a period much smaller than the present day period and a braking index of 3, with no torque decay.
6. We find no significant correlation between velocity and magnetic field estimates. Reconciling this result with previous studies is simple: previous work included strong field and weak field objects that had been spun up by accretion. We found in Paper I that millisecond pulsars are generally a low velocity population. The correlation found in previous work appears to signify only the different evolutionary paths that have led to strong field objects and spun-up, low field objects.
7. Pulsar velocities require some sort of rocket mechanism that augments velocities that would obtain under the condition of symmetric supernovae in binary and nonbinary progenitors. No strong discrimination exists in our analysis for proposed rocket effects

that take place during or shortly after supernova explosions. However, the estimated velocities require a more efficient acceleration mechanism than has been calculated thus far.

8. We suggest that the best means for pushing the limits and testing models is to search for, and measure the proper motions of, pulsars at high galactic latitudes.

Acknowledgements:

We thank Z. Arzoumanian, D. Lorimer, T. Loredo & I. Wasserman for useful discussions. This work was supported by NSF Grants AST-9530397, AST-9528394 and NASA Grant 5-2851. This research was conducted using the resources of the Cornell Theory Center, which receives major funding from the National Science Foundation (NSF) and New York State, with additional support from the Advanced Research Projects (ARPA), the National Center for Research Resources at the National Institutes of Health (NIH), IBM Corporation and other members of the center's Corporate Partnership Program. It was also supported by the National Astronomy and Ionosphere Center, which operates the Arecibo Observatory under a cooperative agreement with the National Science Foundation.

REFERENCES

- Anderson, B. & Lyne, A.G. 1983, *Nature*, 303, 597.
- Arzoumanian, Z., Phillips, J.A., Taylor, J.H. & Wolszczan, A. 1996, *ApJ*, 470, 1111.
- Bailes, M. 1989, *ApJ*, 342, 917
- Bailes, M. *et al.* 1990, *MNRAS*, 247, 322
- Bailes, M., Reynolds, J.E., Manchester, R. N., Kesteven, M.J., & Norris, R.P. 1989, *ApJ*, 343, 53L.
- Bailes, M., Manchester, R. N., Kesteven, M.J., Norris, R.P. & Reynolds, J.E. 1989, *ApJ*, 342, 917.
- Bethe, H. A. 1993, *ApJ*, 412, 192.
- Bhattacharya, D. & van den Heuvel, E. P. J. 1991, *Phys. Rep.* 203, 1.
- Binney, J. & Tremaine, S. 1987, *Galactic Dynamics*, (Princeton: Princeton University Press), p. 17.

- Birkel, M. & Toldrà, R. 1997, astro-ph/9704138
- Bisnovatyi-Kogan, G. S. 1996, in High Velocity Neutron Stars & Gamma-Ray Bursts, eds. R. E. Rothschild & R. E. Lingenfelter, 38.
- Blandford, R. D., Applegate, J. H. & Hernquist, L. 1983, MNRAS, 204, 1025.
- Blaauw, A. 1961 B.A.N. 15, 265.
- Boyd, P.T. *et al.* 1995, ApJ, 448, 365
- Burderi, L., King, A.R., & Wynn, G.A. 1996, MNRAS, 283, L63
- Burrows, A., Hayes, J. & Fryxell, B. A. 1995, ApJ, 450, 330.
- Burrows, A. & Hayes, J 1996, PhysRevLett, 76, 352.
- Camilo, F., Nice, D.J. & Taylor, J.H. *et al.* 1996, ApJ, 461, 812.
- Camilo, F., Thorsett, S. & Kulkarni, S.R. 1994, ApJ, 421, L15.
- Campbell, R.M. *et al.* 1996, ApJ, 461, 95.
- Caraveo, P.A. 1993, ApJ, 415, L111
- Caraveo, P.A. & Bignami, G.F., Mignami, R., Taff, L.G. 1996, ApJ, 461, 91.
- Chernoff, D., Cordes, J. M. and Arzoumanian, Z. 1996, in High Velocity Neutron Stars & Gamma-Ray Bursts, eds. R. E. Rothschild & R. E. Lingenfelter, 16.
- Cordes, J. M. 1986, ApJ, 311, 183.
- Cordes, J. M. 1987, in The Origin & Evolution of Neutron Stars, Proceedings of the 125th Symposium of the IAU held in Nanjing, China, eds. D.J. Helfand & J. H. Huang, 35.
- Cordes, J.M., Romani, R. W. & Lundgren, S. C. 1993, Nature, 362, 133.
- Cordes, J.M. & Chernoff, D. 1997, ApJ, 482, 971 (Paper I).
- Cordes, J. M. & Wasserman, I. 1984, ApJ, 279, 798.
- Cordes, J. M., Wasserman, I & Blaskiewicz, M. 1990, ApJ, 349, 546.
- Cunha, K. & Smith, V. V. 1996, A&A, 309, 892.
- Dewey, R. J. & Cordes, J. M. 1987, ApJ, 321, 780.

- Downs, G. S. & Reichley P. E. 1983, ApJSuppl, 53, 169.
- Fomalont, E. *et al.* 1992, MNRAS, 258, 497.
- Frail, D. A. 1990, PhD Thesis, University of Toronto.
- Frail, D.A. & Weisberg, J. 1990, AJ, 100, 743.
- Frail, D. A., Goss, W. M. & Whiteoak, J. B. Z. 1994, ApJ, 437, 781.
- Frisch, P. C. 1993, Nature, 364, 395.
- Gehrels, N. & Chen, W. 1993, Nature, 361, 706.
- Goldreich, P. & Julian, W. H. 1970, ApJ, 160, 971.
- Goldreich, P., Lai, D. & Sahriling, M. 1997, preprint.
- Goldreich, P. & Reisenegger, A. 1992, ApJ, 395, 250.
- Gott, J. R., Gunn, J. E. & Ostriker, J. P. 1970, ApJ, 160, L91.
- Gunn, J. E. & Ostriker, J. P. 1970, ApJ, 160, 979.
- Gregory, P. C. & Lored, T. J. 1992, ApJ, 398, 146.
- Gwinn, C.R., Taylor, J. H., Weisberg, J.M. & Rawley, L.A. 1986, AJ, 91, 974.
- Halpern, J. P. & Holt, S. S. 1992, Nature, 357, 222.
- Hammersky, P.L., Garzon, F., Mahoney, T., Calbet, X. 1995, MNRAS, 273, 206.
- Harrison, E. R. & Tademaru, E. 1975, ApJ, 201, 447.
- Harrison, P.A., Lyne, A.G. & Anderson, B. 1993, MNRAS, 261, 113
- Heintzmann, H. & Schrufer, E. 1982, A&A, 111, L4
- Helfand, D. J. & Tademaru, E. 1977, ApJ, 216, 842.
- Herant, M., Benz, W. & Colgate, S. 1992, ApJ, 395, 642.
- Horowitz, C. J. & Piekarewicz, J. 1997, hep-ph/9701214.
- Hulse, R. A. and Taylor, J. H. 1975, ApJ, 195, L51.
- Iben, Jr., I. & Tutukov, A. V. 1996, ApJ, 456, 738.

- Itoh, N., Kotouda, T. & Hiraki, K. 1995, ApJ, 455, 244.
- Janka, H. Th. & Müller, E. 1994, A&A, 290, 496.
- Kaspi, V., Manchester, R. N., Siegman, B., Johnston, S. & Lyne, A.G. 1994, ApJ, 422, L83
- Kaspi, V., Bailes, M., Manchester, R.N., Stappers, B.W. & Bell, J.F. 1996, Nature, 381, 584
- Koribalski, B., Johnston, S., Weisberg, J. M. & Wilson, W. 1995, ApJ, 441, 756
- Kulkarni, S. R. 1986, ApJ, 306, L85
- Kusenko, A. & Segrè 1996a, Phys. Rev. Lett. 77, 4872.
- Kusenko, A. & Segrè 1996b, astro-ph/9608103
- Lai, D., Bildsten, L. & Kaspi, V. M. 1995, ApJ, 452, 819
- Leonard, P.J.T. & Tremaine, S. 1990, ApJ, 353, 486.
- Lorimer, D. R., Lyne, A.G. & Anderson, B. 1995, MNRAS
- Lyne, A.G., Anderson, B. & Salter, M. J. 1982, MNRAS, 213, 613.
- Lyne, A.G. & Lorimer, D. R. 1994, Nature, 369, 127.
- Lyne, A.G. & Manchester, R. N. 1988, MNRAS, 234, 477
- Lyne, A.G., Pritchard, R. S. & Graham-Smith, F. 1988, MNRAS, 233, 667
- Lyne, A.G., Pritchard, R. S., Graham-Smith, F. & Camilo, F. 1996, Nature, 381, 497
- Lyne, A.G., Manchester, R. N. & Taylor, J.H. 1985, MNRAS, 213, 613.
- Madau, P. & Blaes, O. 1994, ApJ, 423, 748.
- Manchester, R.N., Newton, L. M. & Durdin, J.M. 1985, Nature, 313, 374
- Manning, R. A., Jeffries, R. D. & Willmore, A. P. 1996, MNRAS, 278, 577.
- Melatos, A. 1997, preprint.
- Michel, F. C. 1969, ApJ, 158, 727.
- Mihalas, D. & Binney, J. 1981, *Galactic Astronomy, Structure and Kinematics*, W. H. Freeman, New York, pp. 382-383.

- Mollerach, S. & Roulet, E. 1997, ApJ, 479, 147.
- Muslimov, A. & Page, D. 1996, ApJ, 458, 347.
- Narayan, R. & Ostriker, J. P. 1990, ApJ, 352, 222.
- Ostriker, J. P. & Gunn, J. E. 1969, ApJ, 157, 1395.
- Paczynski, B. 1990 ApJ, 348, 485.
- Portegies Zwart, S.F. & Verbunt, F. 1996, A&A, 309, 179P.
- Prentice, A. & ter Haar, D. 1969, MNRAS, 146, 423
- Press, W.H., Flannery, B. P., Teukolsky, S. A. & Vetterling, W. T. 1992, *Numerical Recipes in FORTRAN*, 2nd edition, (New York: Cambridge University Press).
- Qian, Y.-Z. 1997, astro-ph/9705055.
- Radhakrishnan, V. & Shukre, C. S. 1985, in *Supernovae: Their Progenitors and Remnants*, ed. G. Srinivasan & V. Radhakrishnan (Bangalore: Indian Acad. Sci), 155.
- Romani, R. W. 1990, Nature, 347, 741
- Rubinstein, R. 1981, *Simulation and the Monte Carlo Method*, John Wiley & Sons, New York.
- Ruderman, M. 1991, ApJ, 366, 261.
- Sang, Y. & Chanmugam, G. 1990, ApJ, 363, 597.
- Shklovskii, I. S. 1970, Astr. Zh., 46, 715.
- Smith, V.V., Cunha, K. & Plez, B. 1994, A&A, 281, L41
- Taam, R.E. & van den Heuvel, E.P.J. 1986, ApJ, 305, 235
- Taylor, J. H. & Cordes, J. M. 1993, ApJ, 411, 674.
- Taylor, J. H., Manchester, R. M., & Lyne, A. G. 1993, ApJS, 88, 529.
- Thompson & Cordova, 1994, ApJ, 421, L13
- Urpin, V. & Geppert, U. 1995, MNRAS, 275, 1117

van den Heuvel, E.P.J. 1993, in Planets around pulsars: Proceedings of the Conference, California Inst. of Technology, 123.

Vivekanand, M. & Narayan, R. 1981, Journal of Astrophysics and Astronomy, 2, 315

Wang, J.C.L. 1996, Nature, 379, 206.

Wang, J.C.L. 1997, preprint.

Wendell, C.E. 1997, ApJ, 333, L95.

Weisberg, J. M., Romani, R. W. & Taylor, J. H. 1989, ApJ, 347, 1030.

Young, E.J. & Chanmugam, G. 1995, ApJ, 442, L53

APPENDIX

A. Individual Objects

Distances, if misestimated by the TC model, are more likely to be overestimated than underestimated because HII regions or other enhancements of the free-electron density will perturb the dispersion measure (DM) upwards. In some cases, the distance estimate can be grossly overestimated.

B0531+21: The Crab pulsar clearly was born near its present z distance from the galactic plane (~ -0.2 kpc). However, its progenitor star may have originated much nearer the plane. Gott *et al.* (1970) argued that the Crab’s progenitor and the 3.75 s pulsar B0525+21 were unbound from the explosion that produced the latter pulsar; the point of origin was the Gem I OB association.

B0540+23: A modest $V_r^{(P)} < 500 \text{ km s}^{-1}$ results if the pulsar was born at $z_0 \sim -0.3$ kpc.

B0630+17: The Geminga pulsar is one of the few with a parallax as well as proper motion measurement. Its speed is modest and the likely range of radial velocities renders unlikely any association with the star λ Ori, which would require a radial velocity of about -700 km s^{-1} (Caraveo *et al.* 1996). A histogram of Monte Carlo values of radial velocity (cf. §5) shows only 0.3% of counts have radial velocity magnitudes as large as 700 km s^{-1} .

B0736–40: The TC model yields only a lower bound on the distance (11.0 kpc) because its DM is too large for its latitude. Using this lower bound, the required radial velocity is $|V_r^{(P)}| > 10^4 \text{ km s}^{-1}$. The distance is likely to be much smaller because an HII region may account for much of DM. Frail (1990) estimates the distance to be only 0.4 kpc based on an analysis of HII regions along the line of sight.

B1508+55: The catalog uncertainty in distance is 60%. The transverse speed exceeds $V_r^{(P)}$ by a factor of 7.

B1642–03: Prentice & ter Haar (1969) first proposed that the DM to this pulsar is contributed to significantly by an HII region. Its distance is then 0.1-0.2 kpc rather than the 1.6 kpc from the TC model. We have used this lower distance range.

B1706–16: Frail (1989) argues that an HII region can account for some of the DM for this pulsar, which might place the pulsar significantly nearer (~ 0.1 kpc) than its

nominal distance, 1.27 kpc. This possibility is less certain than that for B1642–03, so we have used the larger distance.

B1933+16: No auxiliary data contradict the adopted distance or the large transverse speed. The radial velocity need not be large if the birth altitude ~ 0.15 kpc.

B1953+50: The radial velocity exceeds the transverse speed by a factor ~ 3.5 . No auxiliary data contradict the assumed distance. To reduce $|V_r^{(P)}|$ to less than 10^3 or 500 km s^{-1} , the distance would have to be reduced < 1.1 kpc or < 0.54 kpc. Alternatively, for a distance equal to the midpoint, $0.5(D_L + D_U) = 1.84$ kpc, the age must be reduced by a factor $\sim 4 - 6$ to reduce the radial velocity magnitude to 1000 or 500 km s^{-1} .

B2154+40: The radial velocity magnitude is about twice the transverse speed. No auxiliary data exist to contradict the derived distance and velocities.

B2021+51: The parallax from VLBI measurements (Campbell *et al.* 1996) yields a distance consistent with that from the TC model. The spindown age agrees with the kinematic age to better than a factor of two.

B2224+65: The Guitar-Nebula pulsar is the largest, convincing pulsar velocity in excess of 800 km s^{-1} (Cordes, Romani & Lundgren 1993). At the TC distance, the implied radial velocity and birth z are both modest. Evidently, most of the pulsar’s speed is transverse to the line of sight and parallel to the galactic plane. It will escape the Galaxy.

Table 1: Pulsar Proper Motion Data

Name (J2000)	Name (B1950)	ℓ (deg)	b (deg)	μ_α ($\frac{mas}{yr}$)	μ_δ ($\frac{mas}{yr}$)	$\log \tau_S$ (yr)	D_L (kpc)	D_U (kpc)	Ref
0139 + 5814	0136 + 57	129.2	-4.0	-11.0 ± 5.0	-19.0 ± 5.0	5.6	2.22	3.76	1
0332 + 5434	0329 + 54	145.0	-1.2	17.0 ± 1.0	-13.0 ± 1.0	6.7	1.10	1.86	1
0358 + 5413	0355 + 54	148.2	0.8	15.0 ± 10.0	-6.0 ± 10.0	5.8	1.59	2.69	2
0454 + 5543	0450 + 55	152.6	7.5	52.0 ± 6.0	-17.0 ± 2.0	6.4	0.61	1.03	1
0502 + 4654	0458 + 46	160.4	3.1	-8.0 ± 3.0	8.0 ± 5.0	6.3	1.37	2.31	1
0528 + 2200	0525 + 21	-176.1	-6.9	-20.0 ± 19.0	7.0 ± 9.0	6.2	1.75	2.95	1
0534 + 2200	0531 + 21	-175.4	-5.8	-16.0 ± 11.0	-2.0 ± 8.0	3.1	1.54	2.60	3
0543 + 2329	0540 + 23	-175.6	-3.3	19.0 ± 7.0	12.0 ± 8.0	5.4	2.72	4.60	1
0614 + 2229	0611 + 22	-171.2	2.4	-4.0 ± 5.0	-3.0 ± 7.0	5.0	3.63	6.14	1
0629 + 2415	0626 + 24	-171.2	6.2	-7.0 ± 12.0	2.0 ± 12.0	6.6	3.59	6.07	1
0630 - 2834	0628 - 28	-123.0	-16.8	-5.0 ± 18.0	-17.0 ± 26.0	6.4	1.65	2.78	2
0633 + 1746	0630 + 17	-164.9	4.3	138.0 ± 4.0	97.0 ± 4.0	5.5	0.12	0.22	4
0653 + 8051	0643 + 80	133.2	26.8	19.0 ± 3.0	-1.0 ± 3.0	6.7	2.32	3.93	1
0659 + 1414	0656 + 14	-158.9	8.3	64.0 ± 11.0	-28.0 ± 7.0	5.0	0.58	0.99	5
0738 - 4042	0736 - 40	-105.8	-9.2	-80.0 ± 13.0	-3.0 ± 43.0	6.6	0.40	0.80	2
0742 - 2822	0740 - 28	-116.2	-2.4	-29.0 ± 0.9	-0.1 ± 0.4	5.2	1.40	7.70	6
0820 - 1350	0818 - 13	-124.1	12.6	9.0 ± 10.0	-31.0 ± 7.0	7.0	1.89	3.20	1
0826 + 2637	0823 + 26	-163.0	31.7	61.0 ± 3.0	-90.0 ± 2.0	6.7	0.29	0.49	3
0835 - 4510	0833 - 45	-96.4	-2.8	-48.0 ± 2.0	34.9 ± 1.0	4.0	0.39	0.65	6
0837 + 0610	0834 + 06	-140.3	26.3	2.0 ± 5.0	51.0 ± 3.0	6.5	0.55	0.94	3

Table 1: Pulsar Proper Motion Data (continued)

Name (J2000)	Name (B1950)	ℓ (deg)	b (deg)	μ_α ($\frac{mas}{yr}$)	μ_δ ($\frac{mas}{yr}$)	$\log \tau_S$ (yr)	D_L (kpc)	D_U (kpc)	Ref
0908 – 1739	0906 – 17	–113.9	19.9	27.0 ± 11.0	-40.0 ± 11.0	7.0	0.48	0.82	1
0946 + 0951	0943 + 10	–134.6	43.1	-38.0 ± 19.0	-21.0 ± 12.0	6.7	0.75	1.27	3
1136 + 1551	1133 + 16	–118.1	69.2	-102.0 ± 5.0	357.0 ± 3.0	6.7	0.21	0.35	3
1453 – 6413	1449 – 64	–44.3	–4.4	-16.4 ± 1.1	-21.3 ± 0.8	6.0	2.00	5.00	6
1509 + 5531	1508 + 55	91.3	52.3	-73.0 ± 4.0	-68.0 ± 3.0	6.4	1.49	2.51	3
1559 – 4438	1556 – 44	–25.5	6.4	11.0 ± 17.0	20.0 ± 50.0	6.6	1.50	2.50	2
1645 – 0317	1642 – 03	14.1	26.1	41.0 ± 17.0	-25.0 ± 11.0	6.5	0.10	0.50	3
1709 – 1640	1706 – 16	5.8	13.7	75.0 ± 20.0	147.0 ± 50.0	6.2	0.98	1.65	2
1752 – 2806	1749 – 28	1.5	–1.0	-5.0 ± 17.0	8.0 ± 15.0	6.0	1.18	1.99	2
1820 – 0427	1818 – 04	25.5	4.7	3.0 ± 3.0	27.0 ± 3.0	6.2	1.61	2.73	3
1825 – 0935	1822 – 09	21.4	1.3	10.0 ± 19.0	-23.0 ± 19.0	5.4	0.78	1.31	2
1844 + 1454	1842 + 14	45.6	8.1	-9.0 ± 10.0	45.0 ± 6.0	6.5	1.70	2.87	1
1913 – 0440	1911 – 04	31.3	–7.1	7.0 ± 13.0	-5.0 ± 9.0	6.5	2.48	4.19	1
1919 + 0021	1917 + 00	36.5	–6.2	-2.0 ± 30.0	-1.0 ± 10.0	6.4	2.56	4.33	1
1932 + 1059	1929 + 10	47.4	–3.9	79.0 ± 6.0	39.0 ± 4.0	6.5	0.13	0.22	3
1935 + 1616	1933 + 16	52.4	–2.1	2.0 ± 3.0	-25.0 ± 5.0	6.0	6.11	10.32	7
1948 + 3540	1946 + 35	70.7	5.0	-9.0 ± 7.0	-4.0 ± 8.0	6.2	6.05	10.22	1
1955 + 5059	1953 + 50	84.8	11.6	-23.0 ± 5.0	54.0 ± 5.0	6.8	1.37	2.31	1
2022 + 2854	2020 + 28	68.9	–4.7	-9.0 ± 3.0	-13.0 ± 2.0	6.5	1.00	1.69	3
2022 + 5154	2021 + 51	87.9	8.4	-8.1 ± 0.2	13.4 ± 0.2	6.4	0.94	1.59	8

Table 1: Pulsar Proper Motion Data (continued)

Name (J2000)	Name (B1950)	ℓ (deg)	b (deg)	μ_α $(\frac{mas}{yr})$	μ_δ $(\frac{mas}{yr})$	$\log \tau_S$ (yr)	D_L (kpc)	D_U (kpc)	Ref
2048 – 1616	2045 – 16	30.5	–33.1	85.0 ± 16.0	-43.0 ± 17.0	6.5	0.49	0.83	2
2055 + 3630	2053 + 36	79.1	–5.6	-3.0 ± 7.0	3.0 ± 3.0	7.0	4.28	7.23	1
2113 + 2754	2110 + 27	75.0	–14.0	-23.0 ± 2.0	-54.0 ± 3.0	6.9	1.05	1.78	1
2157 + 4017	2154 + 40	90.5	–11.3	18.0 ± 1.0	-3.0 ± 1.0	6.8	4.25	7.19	1
2219 + 4754	2217 + 47	98.4	–7.6	-12.0 ± 8.0	-30.0 ± 6.0	6.5	1.89	3.19	7
2225 + 6535	2224 + 65	108.6	6.8	144.0 ± 3.0	112.0 ± 3.0	6.0	1.54	2.60	1
2354 + 6155	2351 + 61	116.2	–0.2	22.0 ± 3.0	6.0 ± 2.0	6.0	2.53	4.28	1

References: 1. Harrison *et al.* (1992) 2. Fomalont *et al.* (1992) 3. Lyne, Anderson & Salter (1982) 4. Caraveo *et al.* (1996) 5. Thompson & Cordova (1994) 6. Bailes *et al.* (1990) 7. Downs & Reichley (1983) 8. Campbell *et al.* (1996)

Table 2:

Parameter Search Ranges

parameter	units	min	max	range
w_1	—	0	1	$\Delta w_1 = 1$
w_2	—	0	1	$\Delta w_2 = 1$
h_{z1}	kpc	0.01	0.51	$\Delta h_{z1} = 0.5$
h_{z2}	kpc	0.01	0.51	$\Delta h_{z2} = 0.5$
σ_{V1}	km s ⁻¹	25	2025	$\Delta \sigma_{V1} = 2000$
σ_{V2}	km s ⁻¹	200	2000	$\Delta \sigma_{V2} = 1800$
σ_{V3}	km s ⁻¹	100	400	$\Delta \sigma_{V3} = 300$

Table 3: 3D Velocity PDF Models

Model	w_1	w_2	h_{z1}	h_{z2}	σ_{V1}	σ_{V2}	σ_{V3}	N_{parms}	$\log \mathcal{L}L$	Odds
$n_g \cdot n_h$			(kpc)	(kpc)	(km s ⁻¹)	(km s ⁻¹)	(km s ⁻¹)			
<hr/> $\tau_S < 10$ Myr: $N_{psr} = 47$ <hr/>										
1.1	1	—	0.13	—	300	—	—	2	-263.50	1
2.1	0.8	0.2	0.13	—	175	700	—	4	-255.92	10 ^{6.3}
2.2	0.82	0.18	0.13	0.10	175	750	—	5	-255.89	10 ^{5.5}
3.1	0.3	0.15	0.13	—	156	750	200	6	-255.90	10 ^{5.4}
<hr/>										
$\tau_S < 5$ Myr: $N_{psr} = 38$ <hr/>										
1.1	1	—	0.13	—	300	—	—	2	-208.10	1
2.1	0.87	0.13	0.13	—	175	700	—	4	-201.94	10 ^{5.1}
<hr/>										
$\tau_S < 1$ Myr: $N_{psr} = 12$ <hr/>										
1.1	1	—	0.13	—	200	—	—	2	-55.99	1
2.1	0.8	0.2	0.13	—	175	400	—	4	-55.95	0.36
<hr/>										

Table 4:

Best-fit Parameters for Model 2.1

parameter	value	units
w_1	$0.83_{-0.13}^{+0.03}$	—
h_{z1}	$0.13_{-0.03}^{+0.02}$	kpc
σ_{V1}	175_{-26}^{+20}	km s ⁻¹
σ_{V2}	700_{-148}^{+224}	km s ⁻¹

Table 5: Pulsar Velocity Components

Name	V	V_r	$V_{\perp 1}$	$V_{\perp 2}$	z_0
	(km s ⁻¹)				(kpc)
0136 + 57	349 ± 148	-14 ± 249	-139 ± 53	-237 ± 55	-0.10 ± 0.032
0329 + 54	229 ± 111	-24 ± 203	119 ± 19	-91 ± 15	0.01 ± 0.057
0355 + 54	239 ± 141	5 ± 216	139 ± 69	-46 ± 63	0.00 ± 0.078
0450 + 55	263 ± 74	-75 ± 164	191 ± 32	-65 ± 11	-0.11 ± 0.059
0458 + 46	193 ± 96	10 ± 183	-61 ± 24	84 ± 39	0.11 ± 0.054
0525 + 21	290 ± 130	3 ± 204	-209 ± 99	38 ± 68	-0.04 ± 0.163
0531 + 21	221 ± 114	-2 ± 194	-119 ± 75	-13 ± 65	-0.20 ± 0.031
0540 + 23	341 ± 149	3 ± 249	215 ± 73	133 ± 84	-0.25 ± 0.036
0611 + 22	223 ± 120	-16 ± 198	-58 ± 86	-36 ± 114	0.20 ± 0.029
0626 + 24	312 ± 242	71 ± 332	92 ± 86	78 ± 136	0.04 ± 0.168
0628 - 28	349 ± 188	109 ± 289	-141 ± 88	-113 ± 147	-0.05 ± 0.139
0630 + 17	206 ± 92	0 ± 178	113 ± 15	80 ± 11	-0.03 ± 0.006
0643 + 80	274 ± 58	128 ± 77	227 ± 53	-18 ± 37	0.04 ± 0.118
0656 + 14	303 ± 87	16 ± 190	225 ± 44	-101 ± 26	0.09 ± 0.016
0736 - 40	363 ± 220	-250 ± 265	-172 ± 39	107 ± 68	0.15 ± 0.099
0740 - 28	274 ± 72	22 ± 183	-215 ± 15	-1 ± 2	-0.04 ± 0.003
0818 - 13	459 ± 223	184 ± 314	197 ± 65	-284 ± 66	0.03 ± 0.148
0823 + 26	221 ± 33	-20 ± 50	119 ± 21	-178 ± 24	-0.03 ± 0.127
0833 - 45	232 ± 116	21 ± 210	-120 ± 16	87 ± 12	-0.03 ± 0.003
0834 + 06	195 ± 41	58 ± 92	0 ± 15	165 ± 22	0.03 ± 0.112

Table 5: Pulsar Velocity Components (continued)

Name	V	V_r	$V_{\perp 1}$	$V_{\perp 2}$	z_0
	(km s ⁻¹)				(kpc)
0906 – 17	190 ± 55	78 ± 99	98 ± 29	–108 ± 31	0.01 ± 0.125
0943 + 10	358 ± 94	324 ± 79	–114 ± 62	–81 ± 43	0.04 ± 0.122
1133 + 16	466 ± 90	–16 ± 26	–131 ± 19	445 ± 88	0.00 ± 0.123
1449 – 64	342 ± 101	–2 ± 215	–175 ± 17	–223 ± 13	–0.05 ± 0.019
1508 + 55	761 ± 30	118 ± 74	–547 ± 29	–510 ± 26	0.01 ± 0.132
1556 – 44	239 ± 171	21 ± 248	31 ± 91	89 ± 87	0.02 ± 0.146
1642 – 03	194 ± 87	174 ± 98	56 ± 27	–36 ± 18	0.08 ± 0.123
1706 – 16	1186 ± 293	56 ± 728	405 ± 108	856 ± 232	0.01 ± 0.125
1749 – 28	190 ± 120	–6 ± 202	19 ± 60	12 ± 77	–0.01 ± 0.111
1818 – 04	323 ± 102	7 ± 207	20 ± 20	263 ± 48	0.04 ± 0.079
1822 – 09	221 ± 151	–12 ± 225	34 ± 75	–91 ± 75	0.04 ± 0.019
1842 + 14	596 ± 308	–348 ± 401	9 ± 44	400 ± 75	–0.11 ± 0.118
1911 – 04	240 ± 114	21 ± 211	98 ± 60	–69 ± 89	–0.03 ± 0.171
1917 + 00	281 ± 182	24 ± 279	109 ± 81	–54 ± 111	–0.03 ± 0.168
1929 + 10	154 ± 82	–30 ± 154	67 ± 10	33 ± 5	0.11 ± 0.039
1933 + 16	1010 ± 309	–102 ± 650	44 ± 97	–801 ± 180	0.15 ± 0.086
1946 + 35	467 ± 266	16 ± 364	–331 ± 148	48 ± 149	0.11 ± 0.174
1953 + 50	1563 ± 231	–1489 ± 227	–171 ± 36	438 ± 63	–0.03 ± 0.131
2020 + 28	181 ± 79	44 ± 163	–52 ± 17	–85 ± 17	–0.08 ± 0.047
2021 + 51	179 ± 67	–35 ± 154	–56 ± 2	92 ± 4	–0.04 ± 0.060

Table 5: Pulsar Velocity Components (continued)

Name	V	V_r	$V_{\perp 1}$	$V_{\perp 2}$	z_0
	(km s ⁻¹)				(kpc)
2045 – 16	319 ± 66	–152 ± 87	236 ± 44	–127 ± 43	0.04 ± 0.115
2053 + 36	234 ± 126	83 ± 214	101 ± 57	41 ± 55	–0.04 ± 0.152
2110 + 27	444 ± 82	–257 ± 96	–142 ± 23	–325 ± 47	0.06 ± 0.116
2154 + 40	1064 ± 212	–942 ± 206	483 ± 77	–79 ± 25	0.04 ± 0.120
2217 + 47	403 ± 160	–106 ± 257	–165 ± 64	–276 ± 51	0.06 ± 0.136
2224 + 65	1647 ± 224	166 ± 560	1218 ± 153	947 ± 135	0.03 ± 0.080
2351 + 61	392 ± 126	24 ± 236	323 ± 53	74 ± 25	–0.04 ± 0.037

Fig. 1.— Z-velocity vs. time for objects moving near the Sun in the Paczynski potential. Curves are shown only for $V_z > 0$.

Fig. 2.— Lines showing most likely values for $V_r^{(P)}$ and z_0 . For three pulsars (B0540+23, B1449-64 and B2224+65), dashed lines indicate the 68% confidence interval.

Fig. 3.— Most likely values for $V_r^{(P)}$ and z_0 for four pulsars using three different values of braking index. Three lines are shown for each value of braking index to designate the peak likelihood and the 68% confidence regions. Heavy solid lines: $n = 4$. Light solid lines: $n = 3$. Long dashed lines: $n = 2.5$. Dotted lines: $n = 2$.

Fig. 4.— Contour plot of the log likelihood function for the single Gaussian model ($n_g.n_h = 1.1$) as a function of the rms velocity and scale height. Contours are spaced by $\log 2$.

Fig. 5.— Contour plots of the log likelihood function for the double Gaussian model ($n_g.n_h = 2.1$) as a function of values for pairs of parameters and for 2D slices through the best-fit model. Contours are spaced by $\log 2$.

Fig. 6.— Marginalized probability density functions for the four parameters of the double Gaussian model, $n_g.n_h = 2.1$.

Fig. 7.— One-dimensional cuts through the likelihood functions for a double-Gaussian velocity pdf where the torque decay time τ_K is allowed to vary for different values of braking index. The heavy solid line for $n = 2.5$ yields the maximum likelihood solution at $\tau_K \sim 3$ Myr. The two heavy dashed lines, for $n = 4$ and 4.5 , yield the maximum likelihood if there is no decay, $\tau_K \rightarrow \infty$.

Fig. 8.— (Top) Cumulative distribution functions for the velocity magnitude at birth using best fit parameter values for models 1.1 (dotted line), 2.1 (heavy solid line), and 3.1 (dashed line). The light solid lines represent model 2.1 evaluated with parameter values that are $\pm 1\sigma$ from the best fit values. The vertical dashed line marks 500 km s^{-1} , the nominal speed of escape from the Galaxy at the solar circle. (Bottom) Differential probability density functions for models 1.1, 2.1 and 3.1 using best fit parameter values .

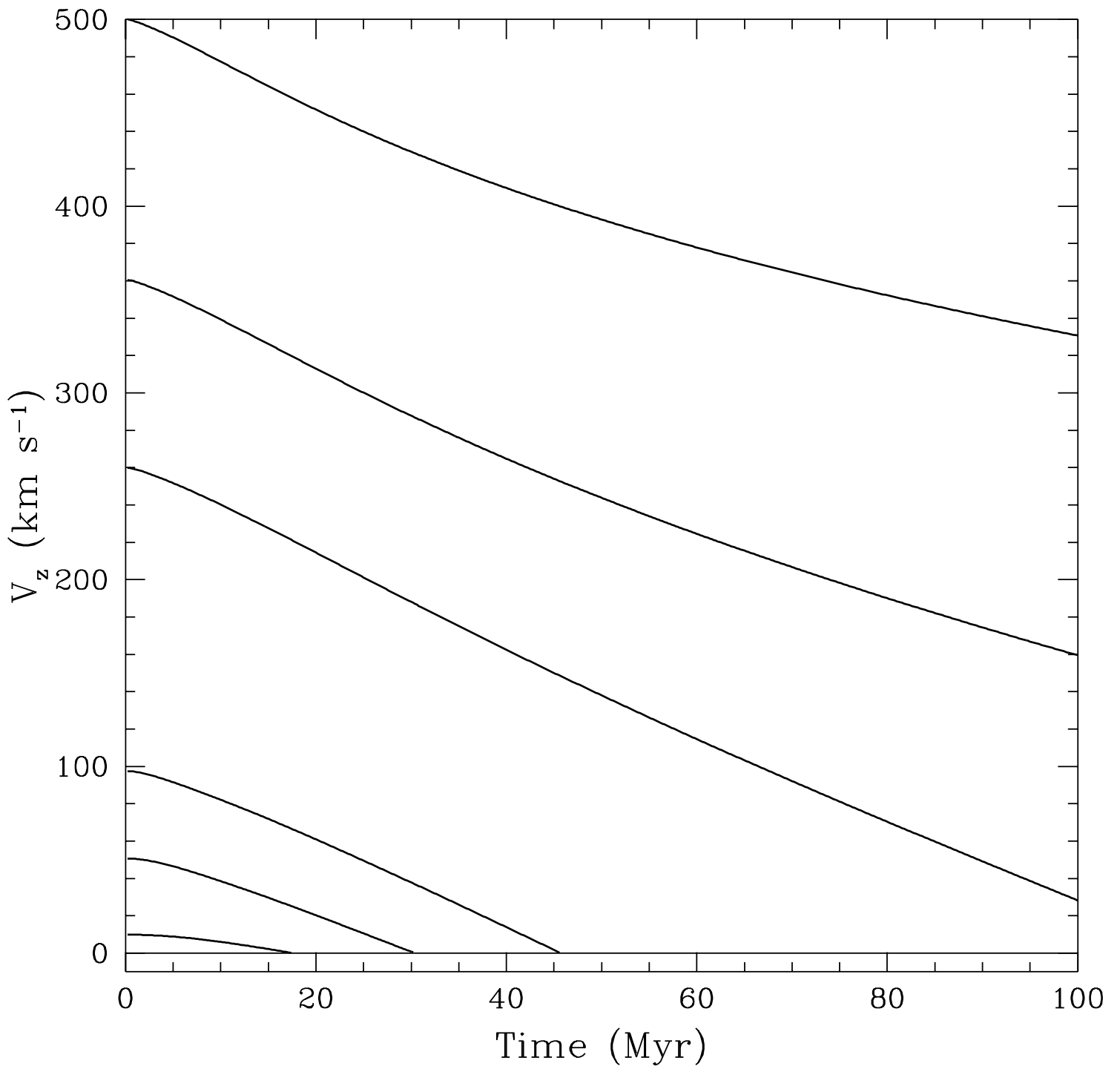
Fig. 9.— Scatter plots of radial velocity $V_r^{(P)}$ against birth altitude, z_0 , and perpendicular speed, V_\perp , for three pulsars. The values result from the Monte Carlo solutions derived using Eq. 32. (a) B1953+50; (b) B2154+40; (c) B2224+65

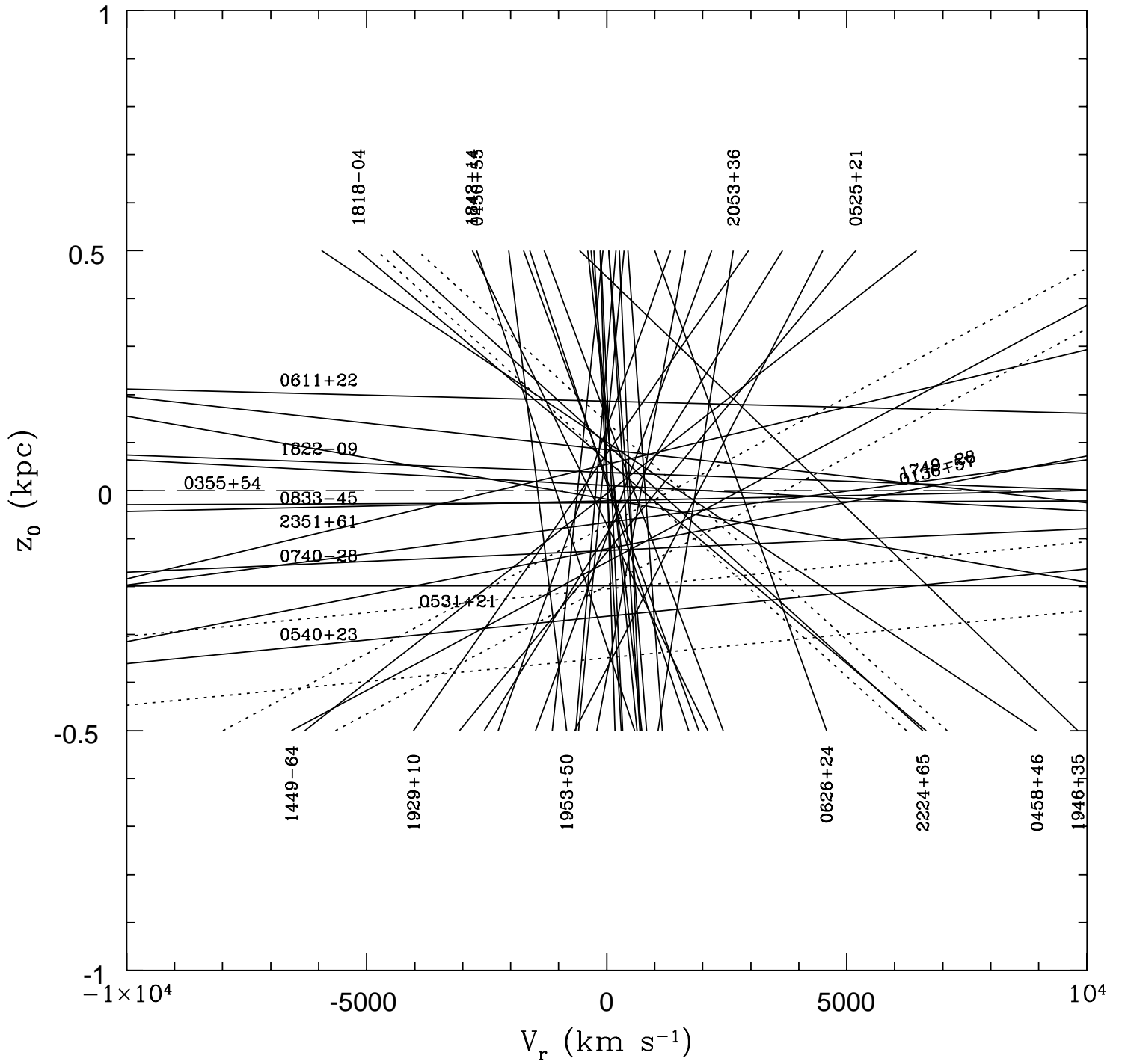
Fig. 10.— Probability density functions and cumulative distribution functions for the ages of three pulsars. Vertical lines indicate the conventional spindown ages obtained from Eq. 2 with a braking index, $n = 3$.

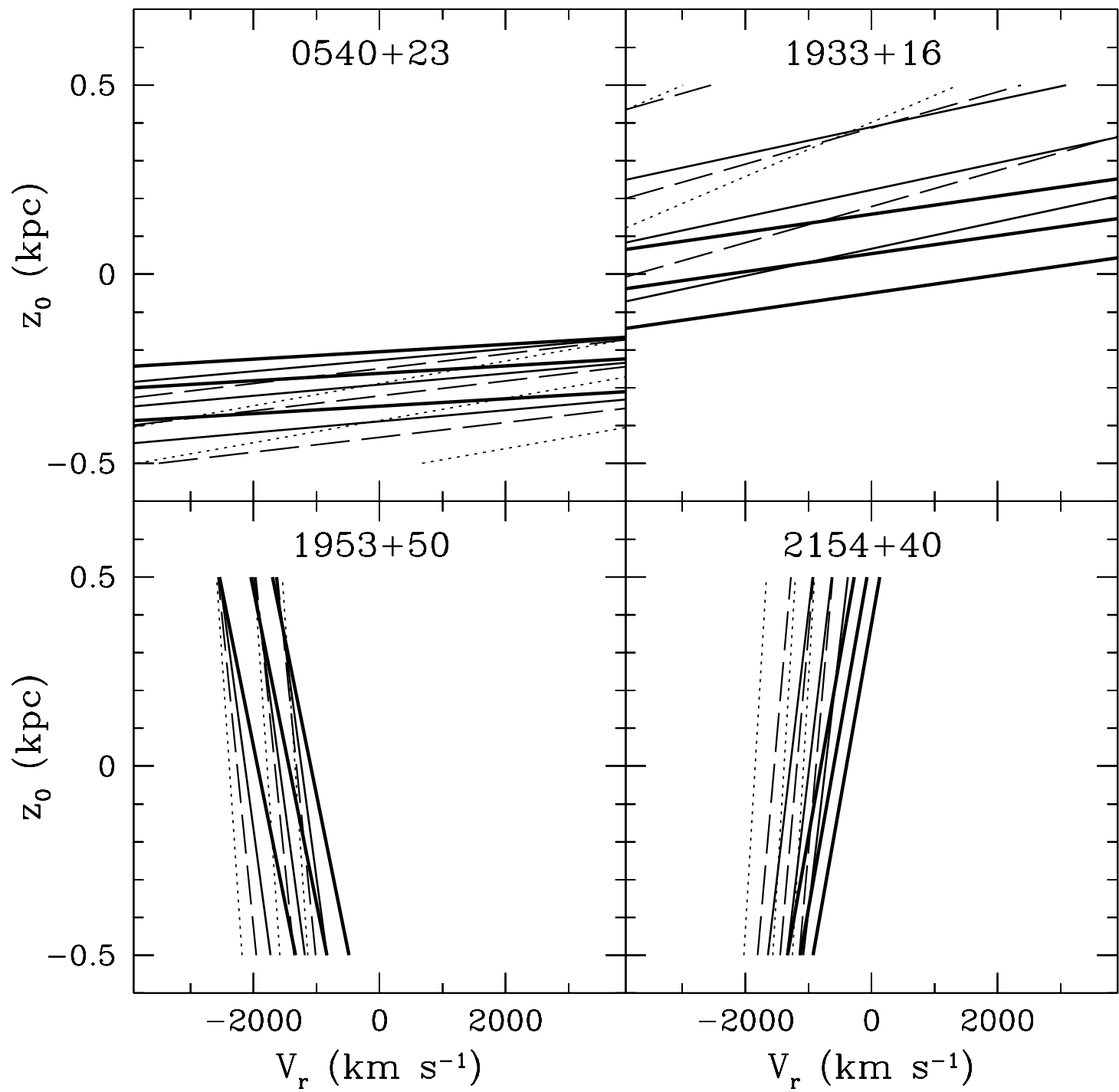
Fig. 11.— Plot showing the acceptable range of possible ages for each of 47 pulsars, calculated using the pdf of Eq. 34. The horizontal line indicates the interval enclosing 68% of the probability. The \times indicates the median of each pdf, the open circle the mode of the pdf, and the solid circle indicates the spindown age $\tau_S \equiv P/2\dot{P}$. For the Crab and Vela pulsars, the kinematic age is unconstraining because of their young ages; for them, we show only their spindown times.

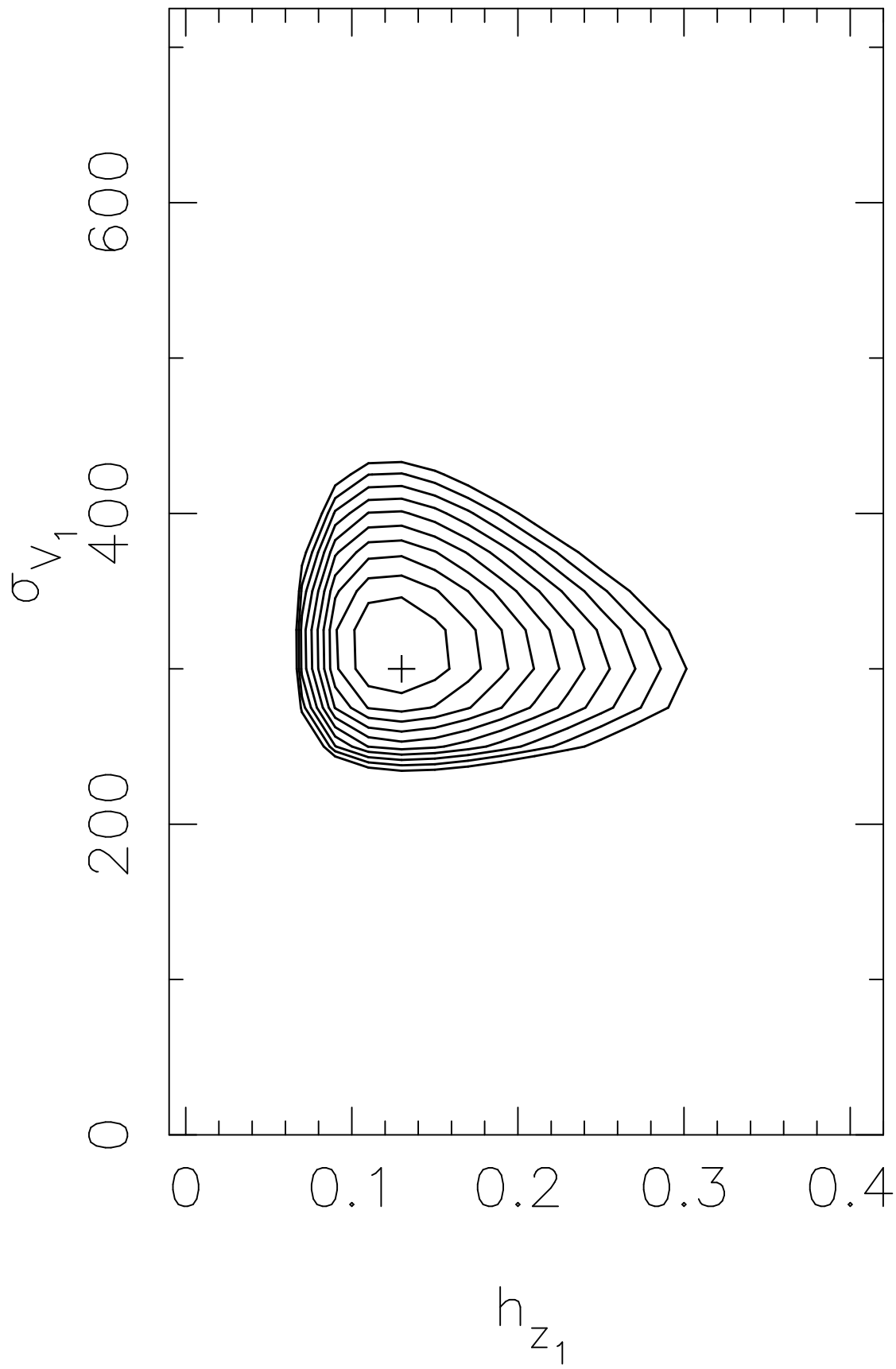
Fig. 12.— Probability density for the ratio of pulsar age to spindown age, $r \equiv t/\tau_S$, based on the individual pdfs for 45 pulsars. The Crab and Vela pulsars have been excluded from our sample because their kinematic ages are poorly constrained.

Fig. 13.— Plot of correlation coefficient between $\log V$ and $\log P^\alpha \dot{P}^\beta$ vs. β .

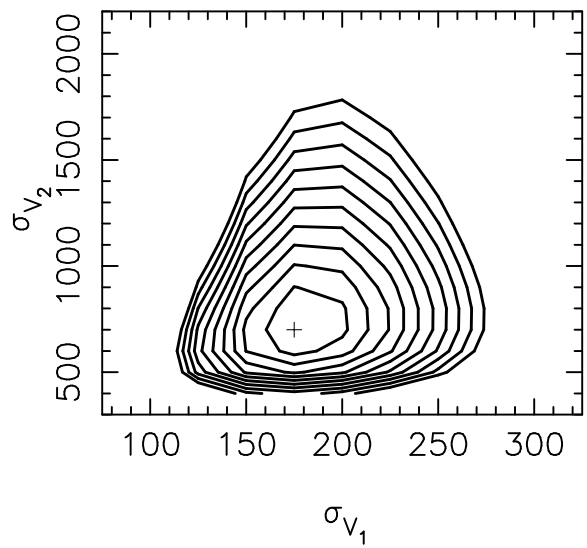
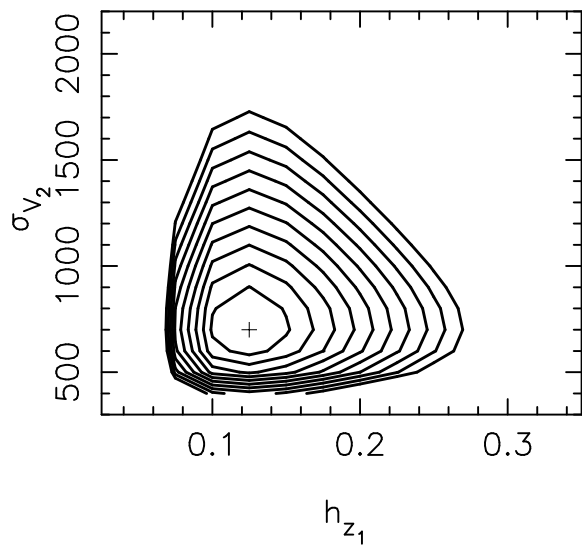
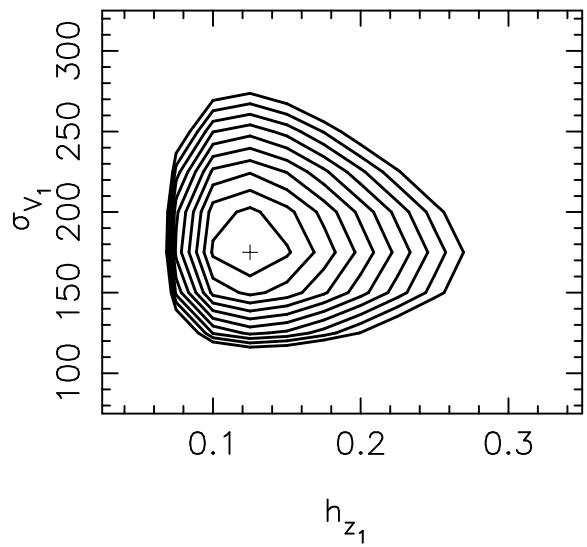
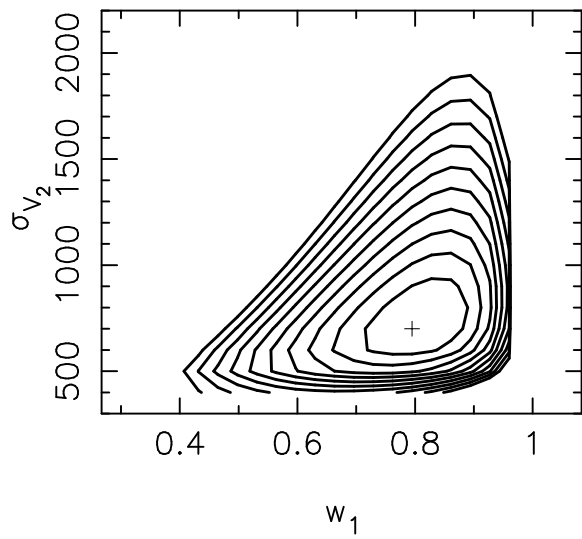
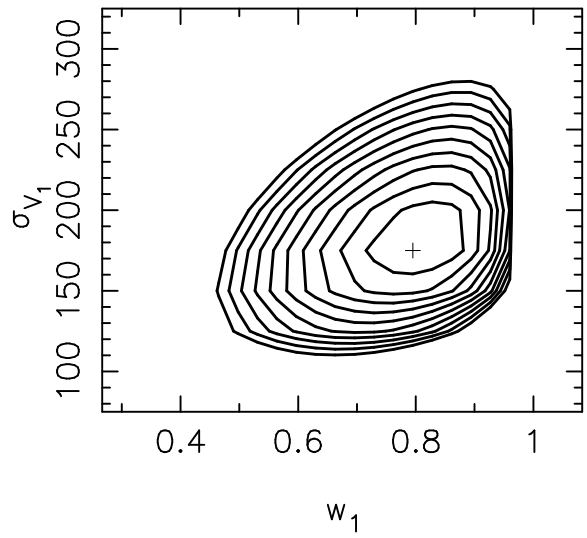
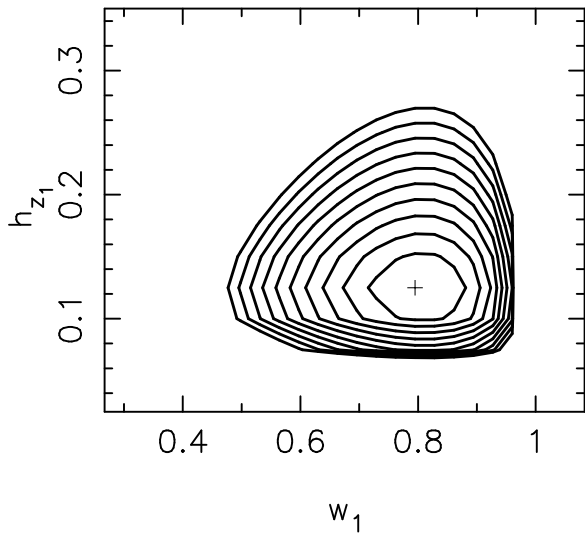


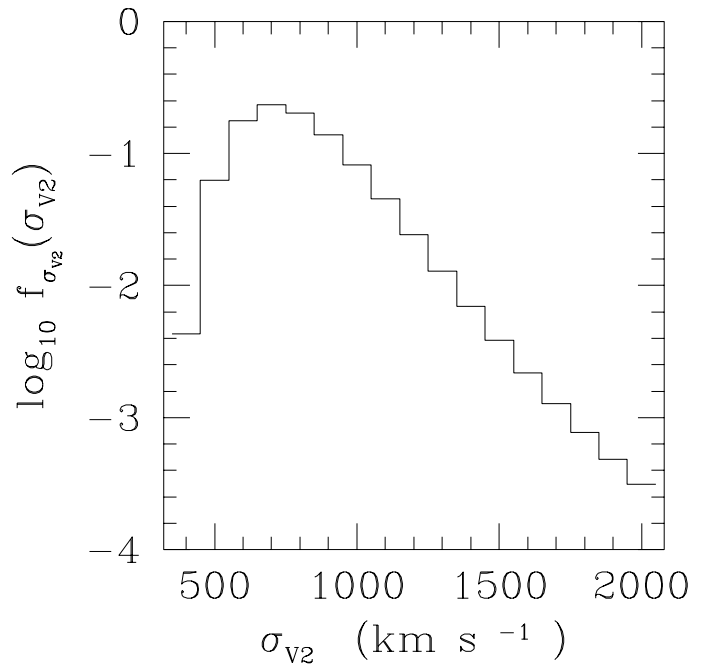
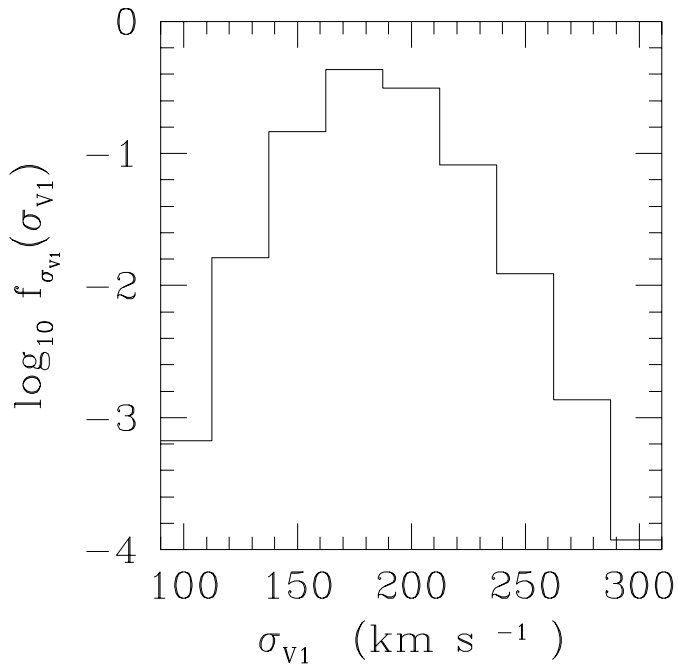
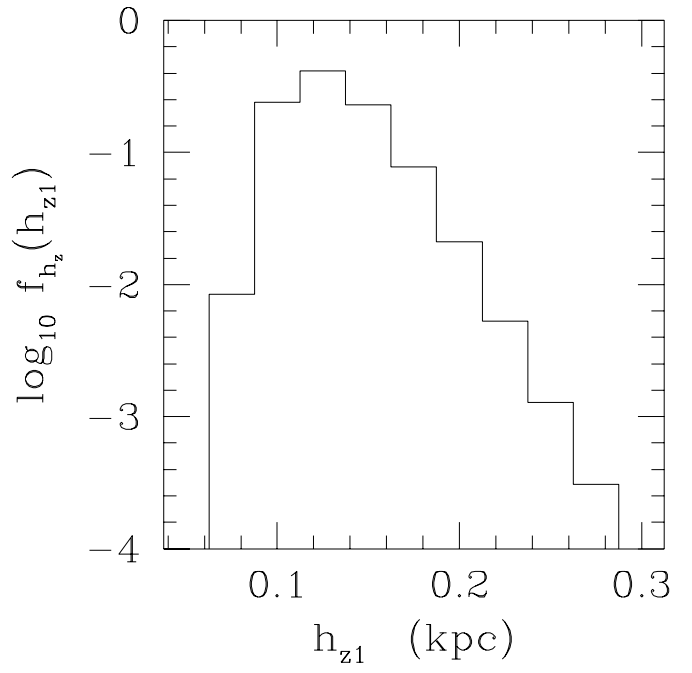
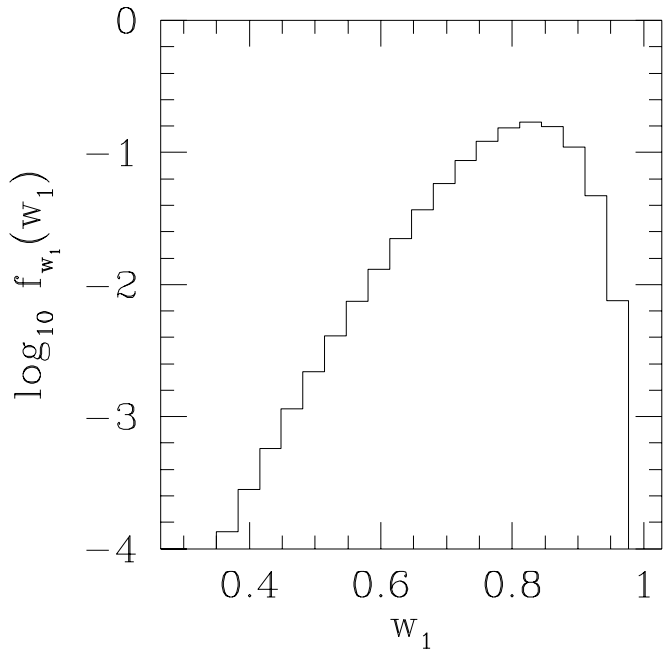


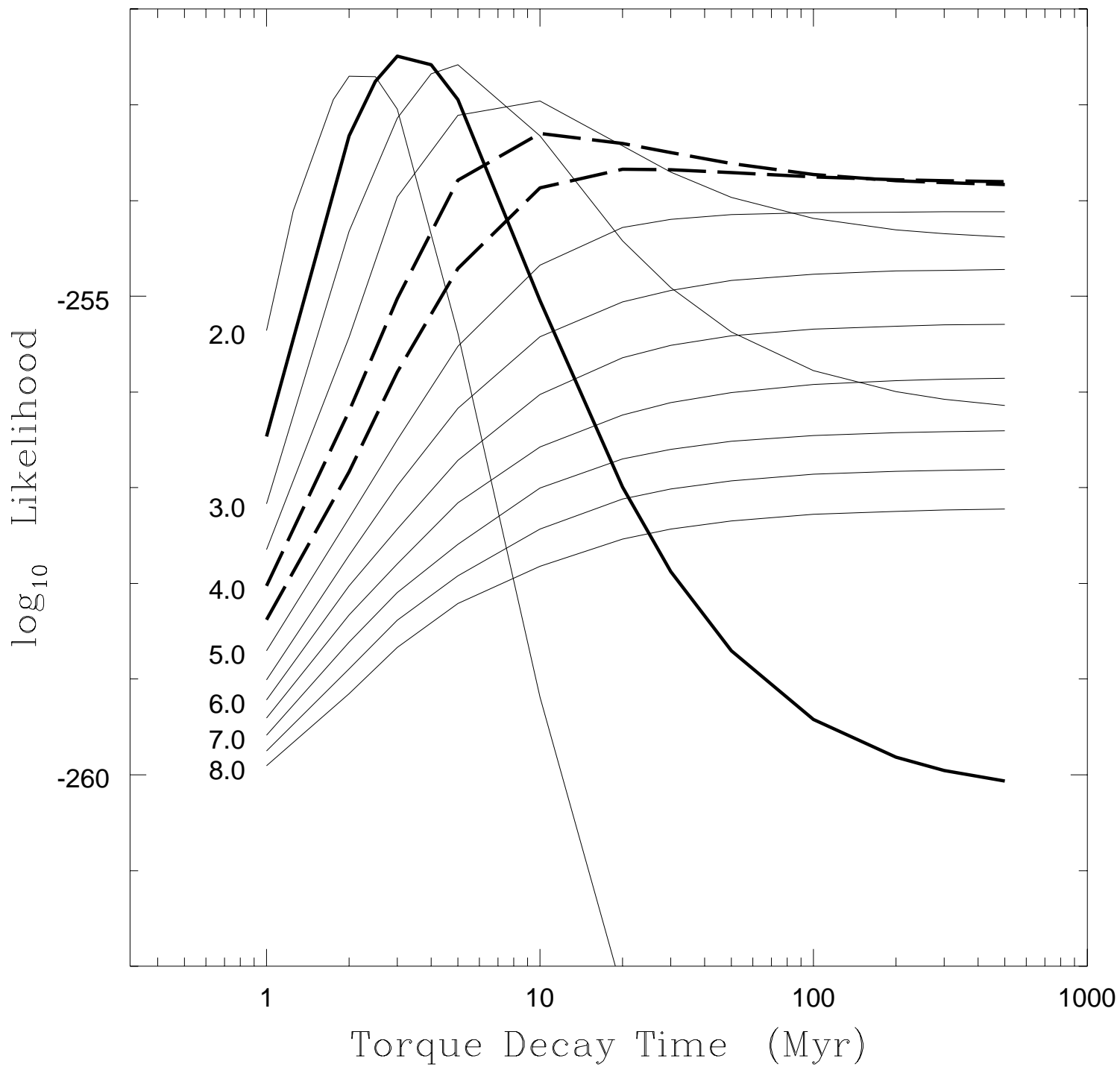


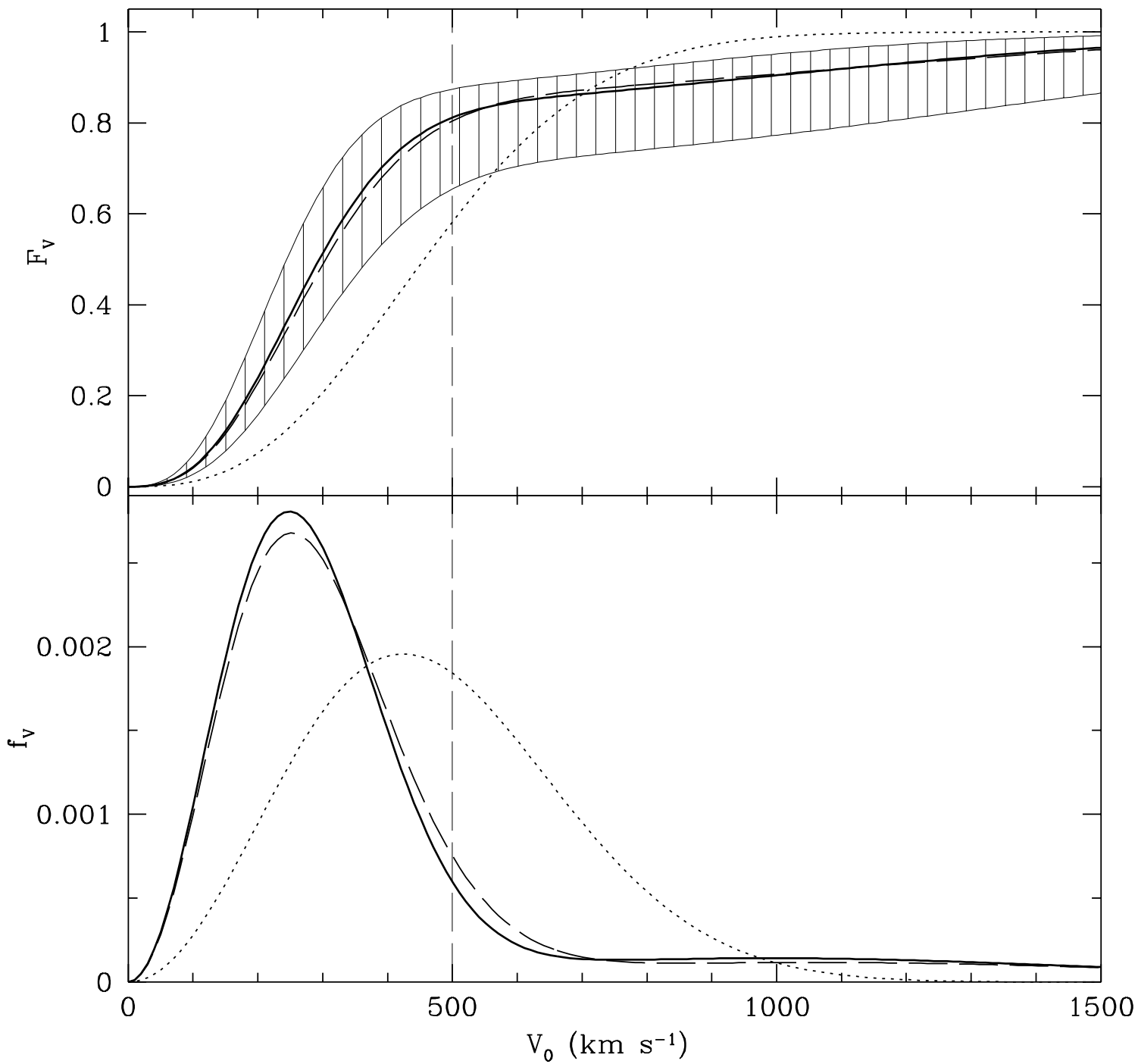


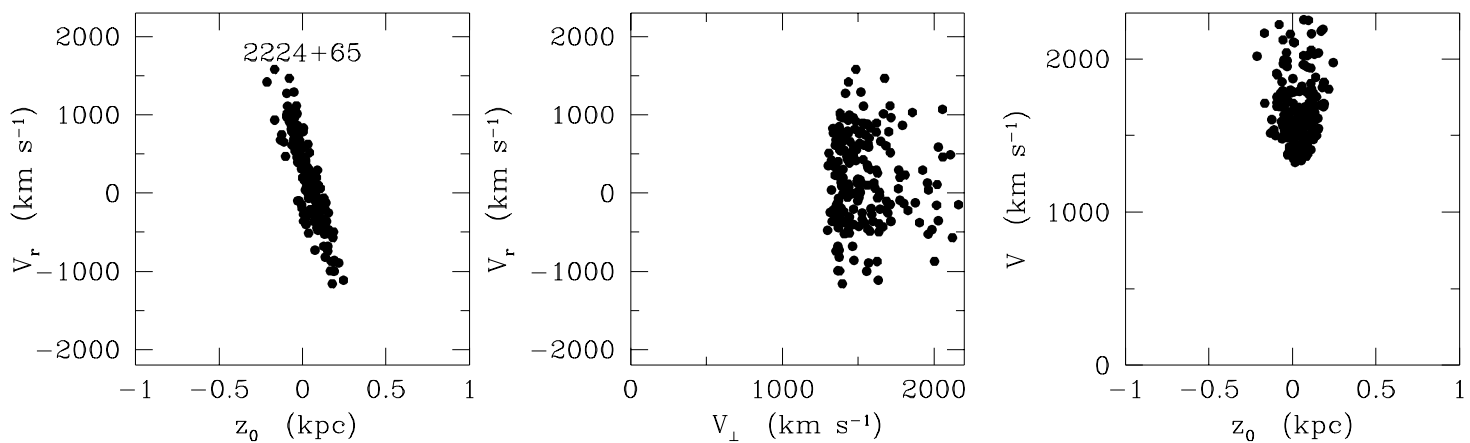
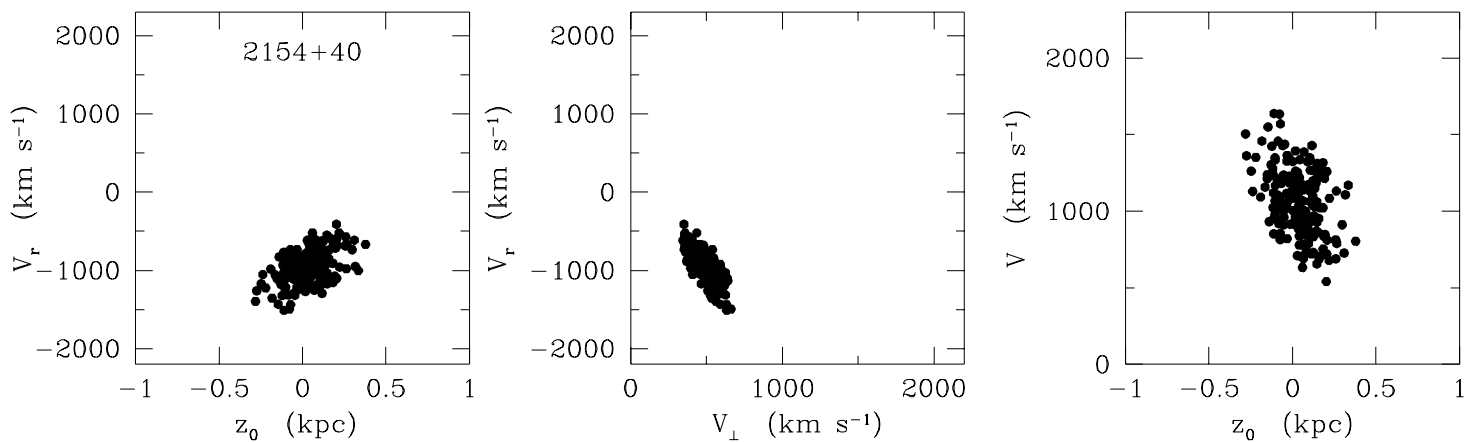
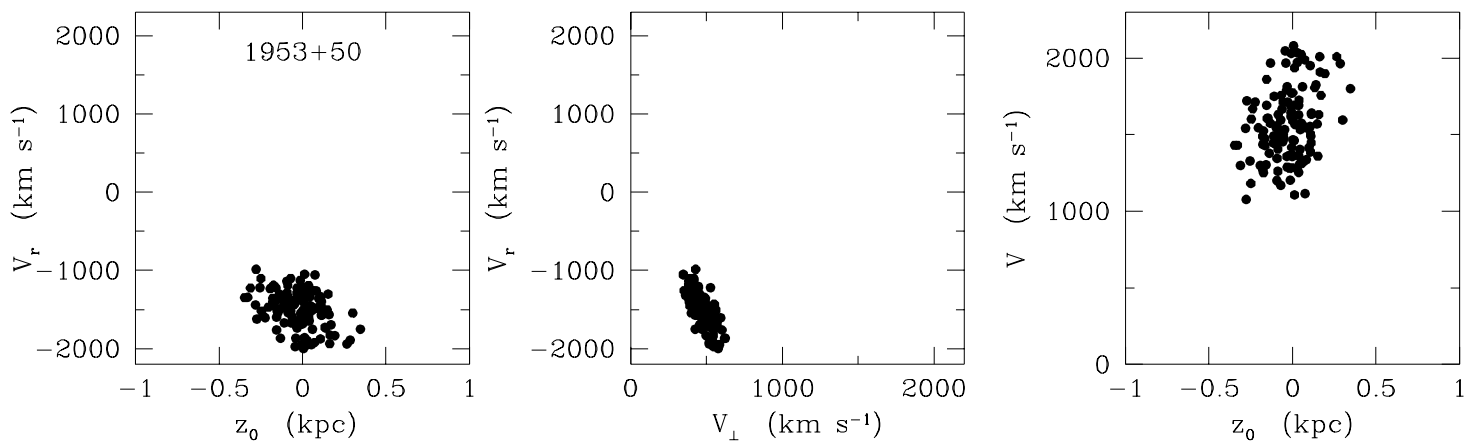
Log likelihood = -255.924

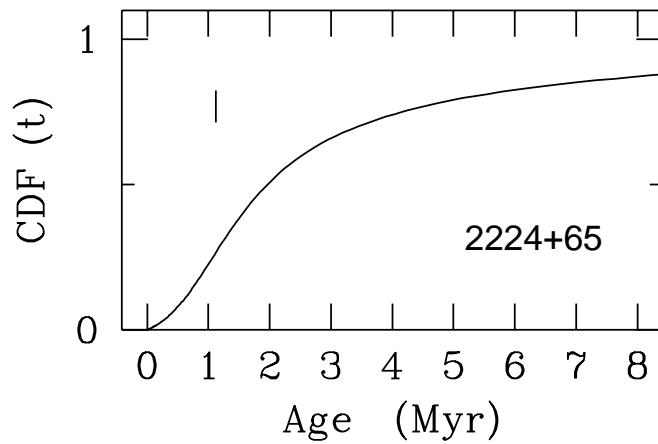
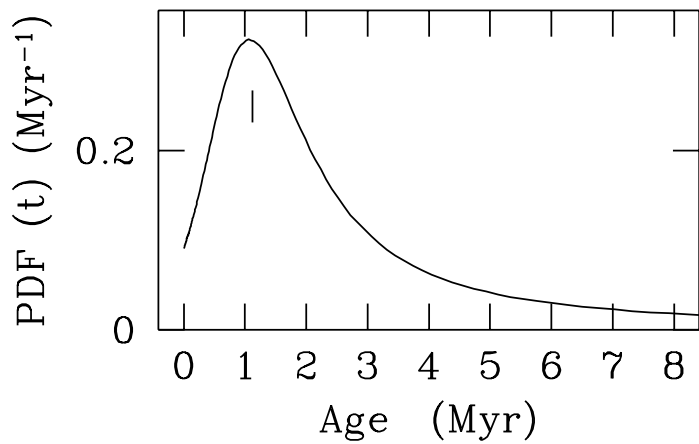
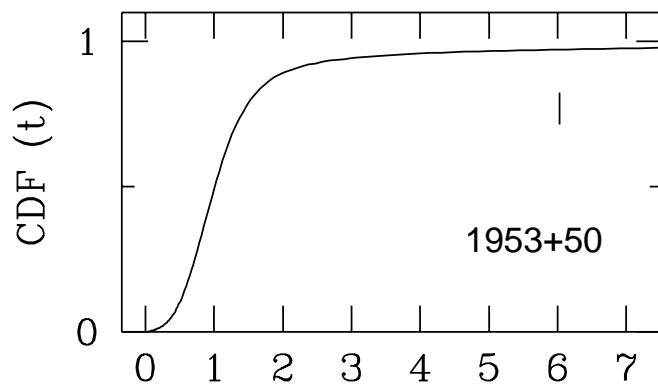
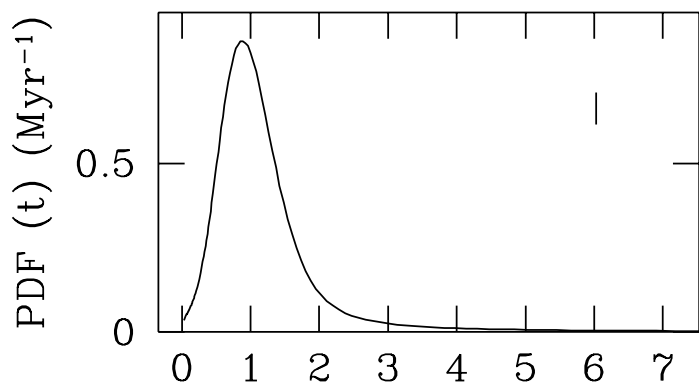
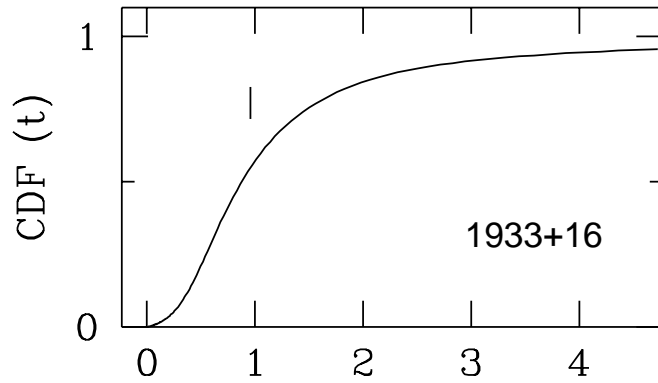
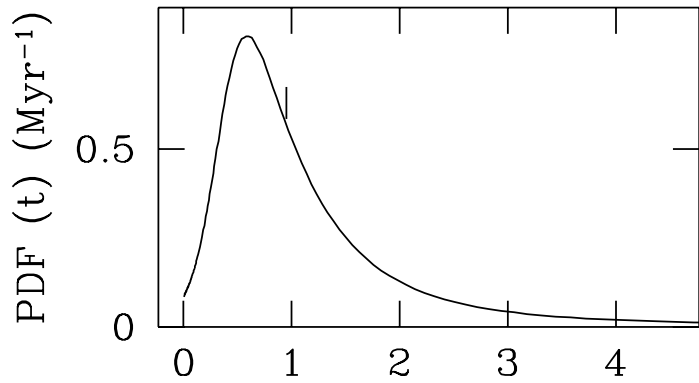












PULSAR

